Chapter 7

Asymptotic theory of stellar oscillations

In Chapter 5 I discussed in a qualitative way how different modes of oscillation are trapped in different regions of the Sun. However, the simplified analysis presented there can, with a little additional effort, be made more precise and does in fact provide quite accurate quantitative information about the oscillations.

The second-order differential equation (5.17) derived in the previous chapter cannot be used to discuss the eigenfunctions. Thus in Section 7.1 I derive a more accurate second-order differential equation for ξ_r. In Section 7.2 the asymptotic solution of such equations by means of the JWKB method is briefly discussed, with little emphasis on mathematical rigour; the results are used to obtain asymptotic expressions for the eigenfrequencies and eigenfunctions. They are used in Sections 7.3 and 7.4 to discuss p and g modes. This approximation, however, is invalid near the surface, and furthermore suffers from critical points in the stellar interior where it formally breaks down. In Section 7.5 I discuss an asymptotic formulation derived by D. O. Gough (*cf.* Deubner & Gough 1984) that does not suffer from these problems; in particular, it incorporates the atmospheric behaviour of the oscillations analyzed in Section 5.4. On the other hand, it uses a dependent variable with a less obvious physical meaning. This method gives a unified asymptotic treatment of the oscillations throughout the Sun, although still under certain simplifying assumptions. A similar, but even more complete, treatment was developed by Gough (1993), although this appears so far not to have been substantially applied to numerical calculations.

One of the most important results of the asymptotic analysis is the so-called *Duvall relation*, which was first discovered by Duvall (1982) from analysis of observed frequencies of solar oscillation. A rough justification for the relation is given in Section 7.3, and a more rigorous derivation is presented in Section 7.5. It is shown that frequencies of p modes approximately satisfy

$$\int_{r_\mathrm{t}}^{R} \left(1 - \frac{L^2c^2}{\omega^2 r^2}\right)^{1/2} \frac{\mathrm{d}r}{c} = \frac{[n + \alpha(\omega)]\pi}{\omega} \,. \tag{7.1}$$

This is evidently a very special dependence of the frequencies on n and l. As discussed in Section 7.7, this relation gives considerable insight into the dependence of the frequencies on the sound speed, and it provides the basis for approximate, but quite accurate, methods for inferring the solar internal sound speed on the basis of observed frequencies.

7.1 A second-order differential equation for ξ_r

To obtain this equation I go back to the two equations (5.12) and (5.13) in the Cowling approximation. By differentiating equation (5.12) and eliminating $\mathrm{d}p'/\mathrm{d}r$ using equation (5.13) we obtain

$$\begin{aligned}\frac{\mathrm{d}^2\xi_r}{\mathrm{d}r^2} &= -\left(\frac{2}{r}-\frac{1}{\Gamma_1}H_p^{-1}\right)\frac{\mathrm{d}\xi_r}{\mathrm{d}r}-\left[-\frac{2}{r^2}-\frac{\mathrm{d}}{\mathrm{d}r}\left(\frac{1}{\Gamma_1}H_p^{-1}\right)\right]\xi_r \\ &\quad +\frac{1}{\rho c^2}\left(\frac{S_l^2}{\omega^2}-1\right)\left\{\rho(\omega^2-N^2)\xi_r-\frac{1}{\Gamma_1}H_p^{-1}p'\right. \\ &\quad \left.+\left[\frac{\mathrm{d}}{\mathrm{d}r}\ln\left|\frac{1}{\rho c^2}\left(\frac{S_l^2}{\omega^2}-1\right)\right|\right]p'\right\}\ . \end{aligned} \tag{7.2}$$

Here p' may be expressed in terms of ξ_r and its derivative by means of equation (5.12). The result is

$$\begin{aligned}\frac{\mathrm{d}^2\xi_r}{\mathrm{d}r^2} &= -\left(\frac{2}{r}-\frac{1}{\Gamma_1}H_p^{-1}\right)\frac{\mathrm{d}\xi_r}{\mathrm{d}r} \\ &\quad +\left[-\frac{1}{\Gamma_1}H_p^{-1}+\frac{\mathrm{d}}{\mathrm{d}r}\ln\left|\frac{1}{\rho c^2}\left(\frac{S_l^2}{\omega^2}-1\right)\right|\right]\frac{\mathrm{d}\xi_r}{\mathrm{d}r} \\ &\quad +[-K(r)+\tilde{h}(r)]\xi_r\ , \end{aligned} \tag{7.3}$$

where K is still given by equation (5.21). All other terms in ξ_r are lumped together in $\tilde{h}$; these contain derivatives of equilibrium quantities, and so may be assumed to be negligible compared with K (except, as usual, near the surface). Equation (7.3) may also be written as

$$\frac{\mathrm{d}^2\xi_r}{\mathrm{d}r^2}-\frac{\mathrm{d}\ln f}{\mathrm{d}r}\frac{\mathrm{d}\xi_r}{\mathrm{d}r}+[K(r)-\tilde{h}(r)]\xi_r=0\ , \tag{7.4}$$

where

$$f(r)=\frac{1}{\rho r^2c^2}\left|\frac{S_l^2}{\omega^2}-1\right|\ . \tag{7.5}$$

It should be noticed that the principal difference between equation (7.4) and equation (5.20) derived previously is the presence of a term in $\mathrm{d}\xi_r/\mathrm{d}r$. This occurs because I have now not neglected the term in ξ_r on the right-hand side of equation (5.12), and the corresponding term in p' in equation (5.13). These terms cannot be neglected if ξ_r is rapidly varying, as assumed.

It is convenient to work with an equation without a first derivative, on the form of equation (5.20). I introduce $\hat{\xi}_r$ by

$$\xi_r(r)=f(r)^{1/2}\hat{\xi}_r(r)\ ; \tag{7.6}$$

$\hat{\xi}_r$ satisfies

$$\frac{\mathrm{d}^2\hat{\xi}_r}{\mathrm{d}r^2}+[K(r)-h(r)]\hat{\xi}_r=0\ , \tag{7.7}$$

where

$$h(r)=\tilde{h}(r)-\frac{1}{2}\frac{\mathrm{d}^2\ln f}{\mathrm{d}r^2}+\frac{1}{4}\left(\frac{\mathrm{d}\ln f}{\mathrm{d}r}\right)^2\ . \tag{7.8}$$

Here h, like $\tilde{h}$, is generally small compared with K. When it is neglected asymptotically, equation (7.7) is identical to equation (5.20), apart from the change of the dependent variable. In particular, the trapping properties of the modes, as inferred from this analysis, are the same as obtained previously.

It is obvious that the derivation of equation (7.7) fails near points where $\omega^2 = S_l^2$, and where consequently f has a singular logarithmic derivative. These are the turning points of p modes. This problem can be avoided by deriving instead a second-order differential equation for p' (see Unno *et al.* 1989, Chapter 16); but, hardly surprisingly, this equation has problems at the turning points for the g modes. It is possible to develop a coherent asymptotic theory by suitably combined use of these two equations; a more convenient approach, however, is to use a second-order equation that is valid throughout the model. I return to this in Section 7.5, but base the initial asymptotic analysis on the somewhat simpler equation (7.7).

7.2 The JWKB analysis

To analyze equation (7.7) asymptotically I use the JWKB method (for Jeffreys, Wentzel, Kramers and Brillouin; in fact the method seems to have been first used by Liouville). It is widely used in quantum mechanics (see *e.g.* Schiff 1949, Section 34), and is also described in Unno *et al.* (1989), Chapter 16. It is possible to provide a firm mathematical foundation for the method; knowing that this is so, it is enough here to sketch how it works, without worrying too much about its convergence properties.

The assumption is that the solution varies rapidly compared with equilibrium quantities, *i.e.*, compared with $K(r)$. Thus I write it as

$$\hat{\xi}_r(r) = a(r) \exp[i\Psi(r)] \; , \tag{7.9}$$

where Ψ is rapidly varying, so that the local radial wave number

$$k_r = \frac{\mathrm{d}\Psi}{\mathrm{d}r} \tag{7.10}$$

is large; $a(r)$ is a slowly varying amplitude function. Formally, it is always possible to write the solution in this form. If equation (7.9) is substituted into equation (7.7), neglecting h, one obtains

$$\left(\frac{\mathrm{d}^2 a}{\mathrm{d}r^2} + 2ik_r \frac{\mathrm{d}a}{\mathrm{d}r} + ia \frac{\mathrm{d}k_r}{\mathrm{d}r} - k_r^2 a \right) \exp(i\Psi) = -K(r) a(r) \exp(i\Psi) \; . \tag{7.11}$$

On the left-hand side the dominant term is the one containing k_r^2; to ensure that this term cancels with the right-hand side, k_r must be chosen as

$$k_r(r) = K(r)^{1/2} \; . \tag{7.12}$$

The next-order terms are those in k_r which must cancel. Thus

$$\frac{1}{a}\frac{\mathrm{d}a}{\mathrm{d}r} = -\frac{1}{2}\frac{1}{k_r}\frac{\mathrm{d}k_r}{\mathrm{d}r} \; , \tag{7.13}$$

or, apart from a constant factor,

$$a(r) = |k_r|^{-1/2} = |K(r)|^{-1/4} \; . \tag{7.14}$$

This leaves in equation (7.11) only a term in the second derivative of a. The asymptotic approximation consists of neglecting this term, which by the assumption is small compared with $k_r^2 a$. Then the approximate solution is completely specified by equations (7.12) and (7.14). Since the solution may be chosen to be real, it can be written as

$$\hat{\xi}_r(r) = A\,|K(r)|^{-1/4} \cos\left(\int_{r_0}^{r} K(r')^{1/2}\mathrm{d}r' + \phi\right) , \qquad \text{for} \quad K(r) > 0 , \tag{7.15}$$

or

$$\begin{aligned}\hat{\xi}_r(r) \;=\; & |K(r)|^{-1/4} \left[A_+ \exp\left(\int_{r_0}^{r} |K(r')|^{1/2}\mathrm{d}r'\right) + A_- \exp\left(-\int_{r_0}^{r} |K(r')|^{1/2}\mathrm{d}r'\right)\right] \\ & \text{for} \quad K(r) < 0 ,\end{aligned} \tag{7.16}$$

for some suitable r_0. Here A and ϕ, or A_+ and A_-, are real constants which must be determined from the boundary conditions.

Notice that this solution has the property of being locally exponential where $K < 0$. Thus it is in accordance with the discussion in Section 5.2. On the other hand, it breaks down at the zeros of K; formally this may be seen from the fact that there a, as obtained in equation (7.12), is singular, and its second derivative cannot be neglected in equation (7.11). Thus we need to make a special analysis of the points where $K = 0$. In particular, this is required to connect the solution in the exponential and oscillatory regions, and hence apply the boundary conditions.

I consider a turning point r_1 such that $K(r) < 0$ for $r < r_1$ and $K(r) > 0$ for $r > r_1$. If r_1 is a simple zero for K, close to r_1 we have approximately that

$$K(r) \simeq K_1(r - r_1) , \tag{7.17}$$

where $K_1 > 0$ is a constant. I introduce the new independent variable x by

$$x = K_1^{1/3}(r - r_1) ; \tag{7.18}$$

then the equation for $\hat{\xi}_r$ can be approximated by

$$\frac{\mathrm{d}^2\hat{\xi}_r}{\mathrm{d}x^2} = -x\hat{\xi}_r , \tag{7.19}$$

with the solution

$$\hat{\xi}_r(r) = C_1 \mathrm{Ai}\,(-x) + C_2 \mathrm{Bi}\,(-x) , \tag{7.20}$$

where C_1 and C_2 are constants, and Ai and Bi are the Airy functions (*e.g.* Abramowitz & Stegun 1964).

To be definite, I consider a solution that is trapped in the oscillatory region outside r_1, and hence we need to choose the constants C_1 and C_2 such as to select the solution that decreases exponentially as r decreases beneath r_1. When $x < 0$, and $|x|$ is large, $\mathrm{Ai}\,(-x)$ and $\mathrm{Bi}\,(-x)$ have the following asymptotic behaviour:

$$\begin{aligned}\mathrm{Ai}\,(-x) \;&\simeq\; \frac{1}{2\sqrt{\pi}}\,|x|^{-1/4} \exp\left(-\frac{2}{3}|x|^{3/2}\right) , \\ \mathrm{Bi}\,(-x) \;&\simeq\; \frac{1}{\sqrt{\pi}}\,|x|^{-1/4} \exp\left(\frac{2}{3}|x|^{3/2}\right) .\end{aligned} \tag{7.21}$$

Thus we must require that $C_2 = 0$, and the solution satisfying the boundary condition for $r < r_1$ is therefore

$$\hat{\xi}_r(r) = C_1 \mathrm{Ai}\,(-x)\ . \tag{7.22}$$

We can use this solution to determine the phase ϕ in equation (7.15). For large positive x the asymptotic expansion of $\mathrm{Ai}\,(-x)$ is

$$\mathrm{Ai}\,(-x) \simeq \frac{1}{\sqrt{\pi}}|x|^{-1/4}\cos\left(\frac{2}{3}x^{3/2} - \frac{\pi}{4}\right)\ . \tag{7.23}$$

This must agree with what is obtained from equation (7.15), assuming that there is a region where both this equation and the approximation in equation (7.23) are valid. From the expansion of K in equation (7.17) we obtain

$$\Psi = \int_{r_1}^{r} K(r')^{1/2}\mathrm{d}r' + \phi = \frac{2}{3}x^{3/2} + \phi\ , \tag{7.24}$$

so that equation (7.15) gives

$$\hat{\xi}_r \simeq AK_1^{-1/6}x^{-1/4}\cos\left(\frac{2}{3}x^{3/2} + \phi\right)\ . \tag{7.25}$$

This agrees with equation (7.23) if

$$\phi = -\frac{\pi}{4}\ . \tag{7.26}$$

Sufficiently far from the turning point r_1 the JWKB solution satisfying the boundary conditions at $r = r_1$ is thus

$$\hat{\xi}_r(r) = A_1|K(r)|^{-1/4}\cos\left(\int_{r_1}^{r} K(r')^{1/2}\mathrm{d}r' - \frac{\pi}{4}\right)\ . \tag{7.27}$$

Similarly, if there is an outer turning point at $r = r_2$, so that $K(r) > 0$ for $r < r_2$ and $K(r) < 0$ for $r > r_2$, one finds that the asymptotic solution that is exponentially decaying for $r > r_2$ is

$$\hat{\xi}_r(r) = A_2|K(r)|^{-1/4}\cos\left(\int_{r}^{r_2} K(r')^{1/2}\mathrm{d}r' - \frac{\pi}{4}\right)\ . \tag{7.28}$$

Exercise 7.1:

Verify this.

To obtain the full solution we must match the two separate solutions smoothly at a suitable point between r_1 and r_2, $r = r_{\mathrm{f}}$, say. I define

$$\begin{aligned}\Psi_1 &\equiv \Psi_1(r_{\mathrm{f}}) = \int_{r_1}^{r_{\mathrm{f}}} K(r)^{1/2}\mathrm{d}r - \frac{\pi}{4}\ ,\\ \Psi_2 &\equiv \Psi_2(r_{\mathrm{f}}) = \int_{r_{\mathrm{f}}}^{r_2} K(r)^{1/2}\mathrm{d}r - \frac{\pi}{4}\ .\end{aligned} \tag{7.29}$$

Then the conditions that both $\hat{\xi}_r$ and its first derivative be continuous at $r = r_{\rm f}$ give

$$\begin{aligned} A_1 K(r_{\rm f})^{-1/4} \cos\Psi_1 &= A_2 K(r_{\rm f})^{-1/4} \cos\Psi_2 \ , \\ -A_1 K(r_{\rm f})^{-1/4} \sin\Psi_1 &= A_2 K(r_{\rm f})^{-1/4} \sin\Psi_2 \ . \end{aligned} \tag{7.30}$$

Notice that in the derivative I have neglected terms coming from the differentiation of K; these are small compared with the term included. These linear equations for A_1, A_2 only have a non-trivial solution if their determinant vanishes. This leads to

$$\sin\Psi_1 \cos\Psi_2 + \cos\Psi_1 \sin\Psi_2 = \sin(\Psi_1 + \Psi_2) = 0 \ , \tag{7.31}$$

or

$$\Psi_1 + \Psi_2 = (n-1)\pi \ , \tag{7.32}$$

where n is an integer. Thus

$$\int_{r_1}^{r_2} K(r)^{1/2} {\rm d}r = (n - \frac{1}{2})\pi, \qquad n = 1, 2, \ldots \ . \tag{7.33}$$

Here K depends on the frequency ω; thus equation (7.33) implicitly determines the frequencies of the modes trapped between r_1 and r_2. In addition, we find that $A_1 = A_2$.

We can also find the asymptotic behaviour of the eigenfunctions. From the definition of $\hat{\xi}_r$, equations (7.5) and (7.6), it follows from equation (7.27) that for $r_1 < r < r_2$

$$\begin{aligned} \xi_r(r) &= \tilde{A} \rho^{-1/2} r^{-1} c^{-1} \left| \frac{S_l^2}{\omega^2} - 1 \right|^{1/2} |K(r)|^{-1/4} \cos\left(\int_{r_1}^{r} K(r')^{1/2} {\rm d}r' - \frac{\pi}{4} \right) \\ &= A \rho^{-1/2} r^{-1} c^{-1/2} \left| \frac{S_l^2/\omega^2 - 1}{N^2/\omega^2 - 1} \right|^{1/4} \cos\left(\int_{r_1}^{r} K(r')^{1/2} {\rm d}r' - \frac{\pi}{4} \right) \ , \end{aligned} \tag{7.34}$$

where $A = \tilde{A}\, \omega^{-1/2}$. This expression is clearly valid only at some distance from the turning points, where the asymptotic approximation (7.23) can be used. Thus the apparently singular behaviour in $|\cdots|$ causes no problems.

Notice that in equation (7.34) $c^{-1/2}$ (which is proportional to $T^{-1/4}$) and $|\cdots|^{1/4}$ vary relatively little through the region where the modes are trapped. Thus the variation of ξ_r through the Sun is dominated by $\rho^{-1/2} r^{-1}$. This is the reason why I plotted the eigenfunction in terms of $\rho^{1/2} r \xi_r(r)$ in Figures 5.8 and 5.10.

We can also find the solution in the exponential regions, by using the asymptotic expansion for Ai in equation (7.21). The results are, for the solution corresponding to equation (7.34) in the trapping region

$$\begin{aligned} \xi_r(r) &\simeq \frac{1}{2} A \rho^{-1/2} r^{-1} c^{-1/2} \left| \frac{S_l^2/\omega^2 - 1}{N^2/\omega^2 - 1} \right|^{1/4} \exp\left(- \int_{r}^{r_1} \left| K(r') \right|^{1/2} {\rm d}r' \right) \\ &\qquad \text{for } r < r_1 \ , \end{aligned} \tag{7.35}$$

and

$$\begin{aligned} \xi_r(r) &\simeq \frac{1}{2} A \rho^{-1/2} r^{-1} c^{-1/2} \left| \frac{S_l^2/\omega^2 - 1}{N^2/\omega^2 - 1} \right|^{1/4} \exp\left(- \int_{r_2}^{r} \left| K(r') \right|^{1/2} {\rm d}r' \right) \\ &\qquad \text{for } r > r_2 \ . \end{aligned} \tag{7.36}$$

7.3 Asymptotic theory for p modes

For high frequencies we may, as in Section 5.2, approximate K by

$$K(r) \simeq \frac{1}{c^2}(\omega^2 - S_l^2) \; . \tag{7.37}$$

As discussed previously the theory, as formulated so far, does not provide reflection at the surface. Mathematically, this is expressed by the lack of a turning point near the surface. Also, the formulation fails near the point where $\omega = S_l$ where the neglected term $h(r)$ in (7.8) is singular. Thus equation (7.33) for the eigenfrequencies cannot immediately be used. It is shown in Section 7.5 below that a proper treatment of the surface and the lower turning point leads to an asymptotic behaviour similar to that discussed above; however, the effective phase shift in the equation corresponding to (7.33) is different. Thus the frequencies for the p modes approximately satisfy

$$\int_{r_\mathrm{t}}^{R} (\omega^2 - S_l^2)^{1/2} \frac{\mathrm{d}r}{c} = (n + \alpha)\pi \; , \tag{7.38}$$

where α is a new phase constant, which contains the contribution 1/4 from the inner turning point, and an, as yet unidentified, contribution from the outer turning point. It is convenient to write this equation as

$$\int_{r_\mathrm{t}}^{R} \left(1 - \frac{L^2}{\omega^2}\frac{c^2}{r^2}\right)^{1/2} \frac{\mathrm{d}r}{c} = \frac{(n + \alpha)\pi}{\omega} \; , \tag{7.39}$$

where $L^2 = l(l+1)$. Notice that the left-hand side of this equation is a function of $w = \omega/L$ [it follows from equation (5.28) that r_t is determined by ω/L]; thus equation (7.39) can be written as

$$\frac{\pi(n + \alpha)}{\omega} = F\left(\frac{\omega}{L}\right) \; , \tag{7.40}$$

where

$$F(w) = \int_{r_\mathrm{t}}^{R} \left(1 - \frac{c^2}{r^2 w^2}\right)^{1/2} \frac{\mathrm{d}r}{c} \; . \tag{7.41}$$

The observed and computed frequencies in fact satisfy relations like equation (7.40) quite closely; this was first noticed by Duvall (1982) for the observed frequencies. An example is illustrated in Figure 7.1.

When the function $F(w)$ is known from observations, equation (7.41) can be inverted to determine $c(r)$. I return to this in Section 7.7.

It is instructive to consider a special case of this equation, which is furthermore a reasonable approximation to the Sun. The solar convection zone is approximately adiabatically stratified, so that

$$\frac{\mathrm{d}\ln p}{\mathrm{d}r} = \Gamma_1 \frac{\mathrm{d}\ln \rho}{\mathrm{d}r} \; ; \tag{7.42}$$

here I assume Γ_1 to be constant (this is evidently not true in the ionization zones of H and He, but they only occupy the outer few per cent of the Sun). We may also assume that g is constant. Finally I take as boundary conditions on the equilibrium structure that $p = \rho = 0$ at $r = R$. With these assumptions the sound speed is given by

$$c^2 = \frac{g}{\mu_\mathrm{p}}(R - r) \; , \tag{7.43}$$

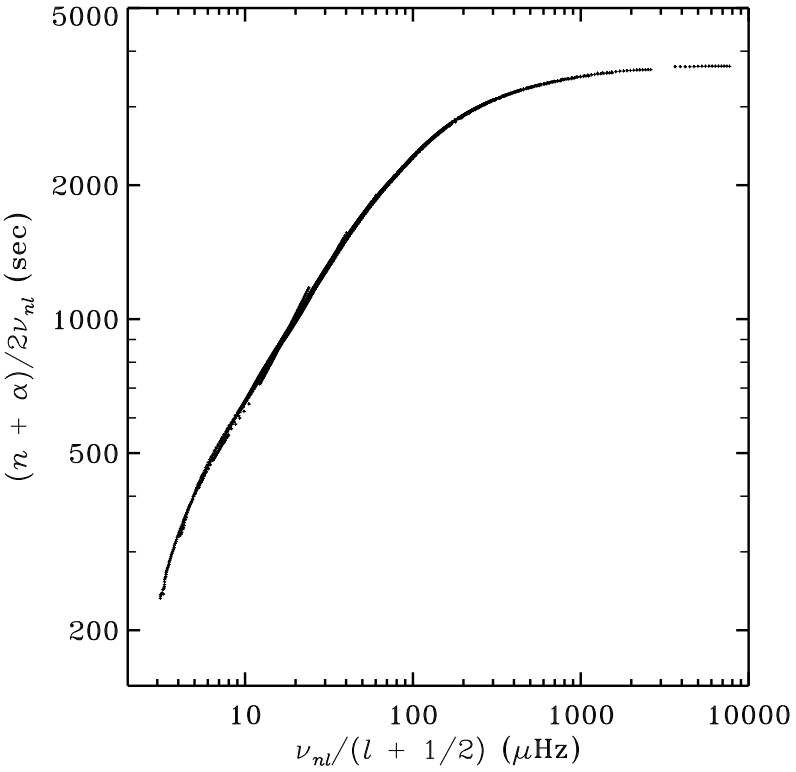

Figure 7.1: Observed frequencies of solar oscillation, plotted according to equation (7.40). The constant value of α, 1.45, was determined such as to minimize the spread in the relation (7.40). (Adapted from Christensen-Dalsgaard *et al.* 1985.)

where $\mu_{\rm p} = 1/(\Gamma_1 - 1)$ is an effective polytropic index of the region considered. I also treat the layer as plane parallel, so that r can be replaced by R in the integral in equation (7.41). Then the integral may easily be evaluated, to yield

$$F(w) = \frac{\pi}{2}\, w\, \frac{\mu_{\rm p} R}{g} \ . \tag{7.44}$$

Exercise 7.2:

Derive equations (7.43) and (7.44).

Thus the dispersion relation (7.40) gives

$$\omega^2 = \frac{2}{\mu_{\rm p}} \frac{g}{R} (n + \alpha) L \ . \tag{7.45}$$

In particular, ω is proportional to $L^{1/2}$. This property is approximately satisfied by the computed (and observed) frequencies at high degree (*cf.* Figure 5.6). Indeed, equation (7.45) might be expected to be approximately valid for modes whose degree is so high that they are entirely trapped within the convection zone.

For modes of low degree, r_t is very close to the centre (see Figure 5.5). In equation (7.39), therefore, the second term in the bracket on the left-hand side is much smaller than unity over most of the range of integration. To exploit this, I consider the difference

$$\begin{aligned} I &= \int_0^R \frac{\mathrm{d}r}{c} - \int_{r_t}^R \left(1 - \frac{c^2}{w^2 r^2}\right)^{1/2} \frac{\mathrm{d}r}{c} \\ &= \int_0^{r_t} \frac{\mathrm{d}r}{c} + \int_{r_t}^R \left[1 - \left(1 - \frac{c^2}{w^2 r^2}\right)^{1/2}\right] \frac{\mathrm{d}r}{c} \\ &\equiv I_1 + I_2 \,, \end{aligned} \tag{7.46}$$

where $w = \omega/L$. Notice that c is almost constant near the centre (it may be shown that the first derivative of c is zero at $r = 0$). Thus I take c to be constant in the first integral, and obtain

$$I_1 = \frac{r_t}{c(0)} \simeq \frac{L}{\omega} = \frac{1}{w} \,, \tag{7.47}$$

by using equation (5.28). In the second integral the integrand is only substantially different from zero for r close to r_t, which was assumed to be small. Thus here I also approximate c by its value at $r = 0$. Furthermore, the upper limit of integration may be replaced by ∞. Then we obtain

$$I_2 = \frac{1}{w} \int_0^1 \left[1 - \left(1 - u^2\right)^{1/2}\right] \frac{\mathrm{d}u}{u^2} = \frac{1}{w} \left(\frac{\pi}{2} - 1\right) \,. \tag{7.48}$$

Thus, finally,

$$I = \frac{1}{w} \frac{\pi}{2} \,, \tag{7.49}$$

and equation (7.39) may be approximated by

$$\int_0^R \frac{\mathrm{d}r}{c} - \frac{L}{\omega} \frac{\pi}{2} = \frac{(n + \alpha)\pi}{\omega} \,, \tag{7.50}$$

or

$$\omega = \frac{(n + L/2 + \alpha)\pi}{\displaystyle\int_0^R \frac{\mathrm{d}r}{c}} \,. \tag{7.51}$$

The derivation of equation (7.51) clearly lacks rigour. However, it may be shown from a more careful asymptotic analysis of the central region (*e.g.* Vandakurov 1967; Tassoul 1980) that the result is correct to leading order, except that L should be replaced by $l + 1/2$. Equation (7.51) may also be written as

$$\nu_{nl} = \frac{\omega_{nl}}{2\pi} \simeq (n + \frac{l}{2} + \frac{1}{4} + \alpha)\Delta\nu \,, \tag{7.52}$$

where

$$\Delta\nu = \left[2 \int_0^R \frac{\mathrm{d}r}{c}\right]^{-1} \tag{7.53}$$

is the inverse of twice the sound travel time between the centre and the surface. This equation predicts a uniform spacing $\Delta\nu$ in n of the frequencies of low-degree modes. Also, modes with the same value of $n + l/2$ should be almost degenerate,

$$\nu_{nl} \simeq \nu_{n-1\,l+2} \ . \tag{7.54}$$

This frequency pattern has been observed for the solar five-minute modes of low degree (*cf.* Chapter 2), and may be used in the search for stellar oscillations of solar type. In fact, as shown in Figure 5.14 it is visible even down to very low radial order for computed frequencies of models near the zero-age main sequence.

The *deviations* from the simple relation (7.52) have considerable diagnostic potential. The expansion of equation (7.39), leading to equation (7.51), can be extended to take into account the variation of c in the core (Gough 1986a); alternatively it is possible to take the JWKB analysis of the oscillation equations to higher order (Tassoul 1980). The result may be written as

$$\nu_{nl} \simeq (n + \frac{l}{2} + \frac{1}{4} + \alpha)\Delta\nu - (AL^2 - \delta)\frac{\Delta\nu^2}{\nu_{nl}} \ , \tag{7.55}$$

where

$$A = \frac{1}{4\pi^2\Delta\nu}\left[\frac{c(R)}{R} - \int_0^R \frac{\mathrm{d}c}{\mathrm{d}r}\frac{\mathrm{d}r}{r}\right] \ . \tag{7.56}$$

Hence

$$\delta\nu_{nl} \equiv \nu_{nl} - \nu_{n-1\,l+2} \simeq -(4l+6)\frac{\Delta\nu}{4\pi^2\nu_{nl}}\int_0^R \frac{\mathrm{d}c}{\mathrm{d}r}\frac{\mathrm{d}r}{r} \ , \tag{7.57}$$

where I neglected the term in the surface sound speed $c(R)$. It is often convenient to represent observed or computed frequencies in terms of a limited set of parameters associated with the asymptotic description of the modes. This may be accomplished by fitting the asymptotic expression to the frequencies. By carrying out a polynomial fit in the quantity $x - x_0$, where $x = n + l/2$ and x_0 is a suitable reference value (Scherrer *et al.* 1983, Christensen-Dalsgaard 1988b) one obtains the average over n of $\delta\nu_{nl}$ as

$$\langle\delta\nu_{nl}\rangle_n \simeq (4l+6)D_0 \ , \tag{7.58}$$

where

$$D_0 \simeq -\frac{1}{4\pi^2 x_0}\int_0^R \frac{\mathrm{d}c}{\mathrm{d}r}\frac{\mathrm{d}r}{r} \ . \tag{7.59}$$

Thus $\delta\nu_{nl}$ is predominantly determined by conditions in the stellar core. Physically, this may be understood from the fact that only near the centre is k_h comparable with k_r. Elsewhere the wave vector is almost vertical, and the dynamics of the oscillations is largely independent of their horizontal structure, *i.e.*, of l; therefore at given frequency the contributions of these layers to the frequency are nearly the same, and hence almost cancel in the difference in equation (7.57).

It should be noted that the accuracy of expressions (7.58) and (7.59) is questionable; they appear to agree fortuitously with frequencies computed for models of the present Sun, whereas they are less successful for models of different ages or masses (Christensen-Dalsgaard 1991a). However, the form of the dependence of $\langle\delta\nu_{nl}\rangle_n$ on l shown in equation (7.58), as well as the argument that this quantity is most sensitive to conditions in stellar cores, probably have a broader range of validity. As a star evolves, the hydrogen abundance

in the core decreases and hence the mean molecular weight increases. For an approximately ideal gas, the sound speed may be obtained from

$$c^2 \simeq \frac{k_{\rm B}T}{\mu m_{\rm u}} \; ; \tag{7.60}$$

since the central temperature varies little during hydrogen burning, due to the strong temperature sensitivity of the nuclear reaction rates, the main effect on the sound speed in the core comes from the change in the mean molecular weight μ. Consequently c decreases as the star evolves, the decrease being most rapid at the centre where hydrogen burning is fastest. As a result, c develops a local minimum at the centre, and $\mathrm{d}c/\mathrm{d}r$ is positive in the core. This region gives a negative contribution to D_0 (*cf.* eq. 7.57), of increasing magnitude with increasing age, and hence D_0 decreases with increasing age (see also Christensen-Dalsgaard 1991a). Hence D_0, which can in principle be observed, is a measure of the evolutionary state of the star. On the other hand, the overall frequency separation $\Delta\nu$, defined in equation (7.53), approximately scales as the inverse of the dynamical time scale which, for main-sequence stars, is largely determined by the mass.

These considerations motivate presenting the average frequency separations in a $(\Delta\nu_0, D_0)$ diagram, as illustrated in Figure 7.2; this is analogous to the ordinary Hertzsprung-Russell diagram. As shown in panel (b) (note the different scales) most of the variation in $\Delta\nu_0$ is in fact related to $t_{\rm dyn}$, such that $\Delta\nu_0$ scales as $M^{1/2}/R^{3/2}$. It is evident from Figure 7.2 that on the assumption that the other parameters of the star (such as composition) are known, a measurement of $\Delta\nu$ and D_0 may allow determination of the mass and evolutionary state of the star (Christensen-Dalsgaard 1984b; Ulrich 1986, 1988; Christensen-Dalsgaard 1988b). On the other hand, Gough (1987) analyzed the sensitivity of this result to the other stellar parameters, and found that the uncertainty in the knowledge of the heavy element abundance, in particular, had a severe effect on the determination of the mass and age. As an example of such sensitivity, Figure 7.2(c) shows the consequences of an increase of the hydrogen abundance by 0.03. A careful analysis of the information content in measured frequency separations, when combined with more traditional measurements of stellar properties, was given by Brown *et al.* (1994).

The eigenfunctions of p modes can be found from equation (7.34). It is convenient to use equation (7.38) to get

$$\int_{r_{\rm t}}^{r} K(r')^{1/2}\mathrm{d}r' = -\int_{r}^{R} K(r')^{1/2}\mathrm{d}r' + (n+\alpha)\pi \; , \tag{7.61}$$

so that we obtain

$$\xi_r(r) \simeq \tag{7.62}$$
$$A\rho^{-1/2}c^{-1/2}r^{-1}\left|1-\frac{S_l^2}{\omega^2}\right|^{1/4}\cos\left[\omega\int_r^R\left(1-\frac{S_l^2}{\omega^2}\right)^{1/2}\frac{\mathrm{d}r'}{c}-(-1/4+\alpha)\pi\right] \; ,$$

where I have again neglected N^2/ω^2. However, the derivation neglects the fact that the present simple asymptotic description breaks down near the lower turning point. As shown in Section 7.5, a more appropriate treatment gives essentially the same result, except that the term $-1/4$ in equation (7.62) must be replaced by $1/4$. Also, to simplify this expression further I note that S_l^2 decreases quite rapidly with increasing r. Near $r = r_{\rm t}$, ω^2 and S_l^2 are

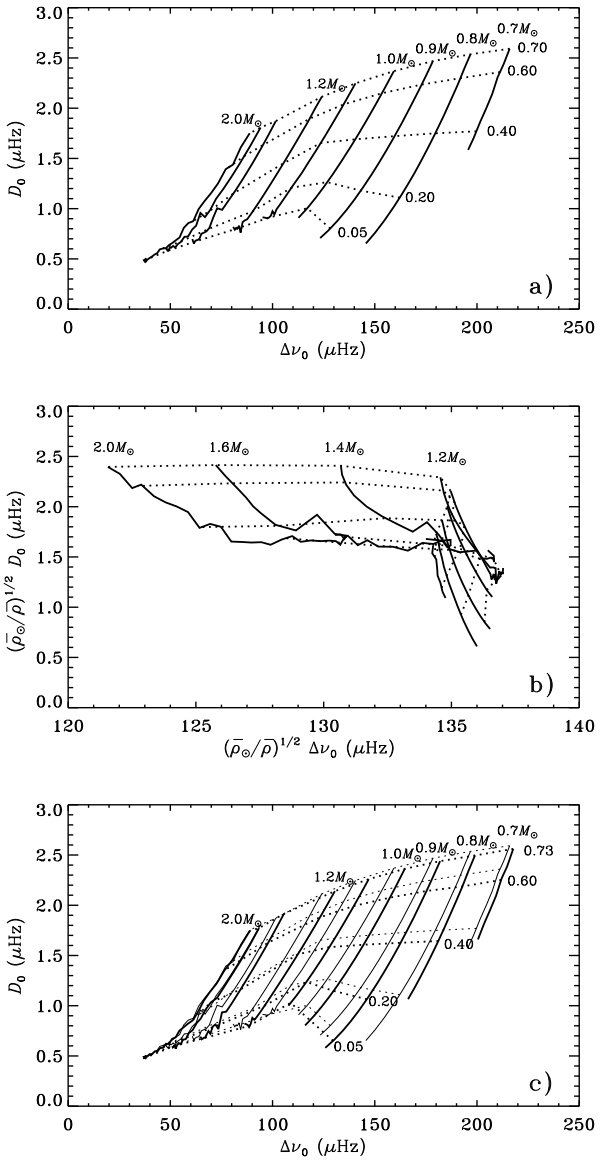

Figure 7.2: Evolution tracks (————) and curves of constant central hydrogen abundance (·····) in $(\Delta\nu_0, D_0)$ diagrams. Here $\Delta\nu_0$ is the average separation between modes of the same degree and adjacent radial order, and D_0 is related to the small separation between ν_{nl} and $\nu_{n-1\,l+2}$ (*cf.* eq. 7.58). The stellar masses, in solar units, and the values of the central hydrogen abundance, are indicated. In panel (b), the frequency separations have been scaled by $(\overline{\rho})^{-1/2}$ ($\overline{\rho} \propto M/R^3$ being the mean density), to take out the variation with $t_{\rm dyn}^{-1}$. Panel (c) shows the effect of increasing the hydrogen abundance by 0.03 (heavy lines), relative to the case presented in panel (a) (shown here with thin lines). (From Christensen-Dalsgaard 1993b.)

comparable, but at some distance from the turning point we can assume that $S_l^2/\omega^2 \ll 1$. Here, therefore

$$\xi_r(r) \simeq A\rho^{-1/2}c^{-1/2}r^{-1}\cos\left[\omega\int_r^R \frac{\mathrm{d}r'}{c} - (1/4+\alpha)\pi\right] . \tag{7.63}$$

To this approximation the eigenfunction is independent of l. Oscillations with the same frequency but different l therefore have approximately the same eigenfunctions near the surface, if they are normalized to the same surface value. This was also seen in Figure 5.8. This property is important for the interpretation of the observed frequencies. It may be understood physically in the following way: near the surface the vertical wavelength is much shorter than the horizontal wavelength (*i.e.*, $k_r \gg k_\mathrm{h}$); the tangential component of the displacement therefore has essentially no influence on the dynamics of the oscillation, which is consequently independent of l.

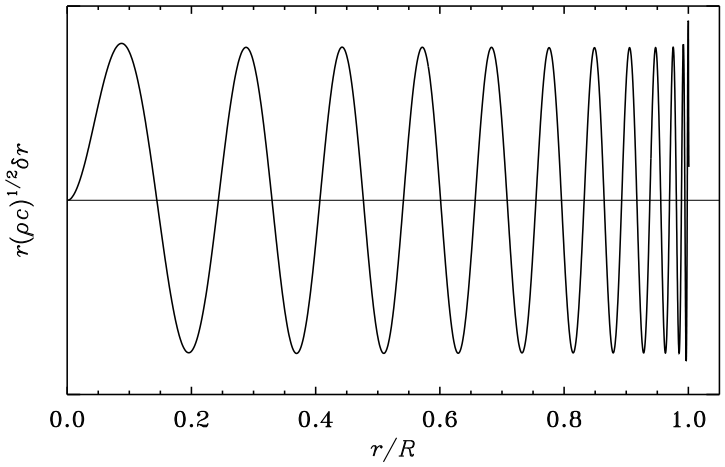

Figure 7.3: Scaled eigenfunction for radial p mode of order $n = 23$ and frequency $\nu = 3310\,\mu$Hz in a normal solar model (the same mode as was shown in Figure 5.8a). According to the asymptotic equation (7.63) the quantity plotted should oscillate between fixed limits in the region where the mode is trapped.

From equation (7.63) one should expect that $c^{1/2}\rho^{1/2}r\,\xi_r(r)$ behaves like a cosine function with a non-uniform argument. This is confirmed to high accuracy by Figure 7.3. Thus equation (7.63) in fact gives a reasonable description of the eigenfunctions of high-order p modes in the region where they are trapped.

7.4 Asymptotic theory for g modes

For these in general $\omega^2 \ll S_l^2$, and I approximate K by

$$K(r) \simeq \frac{l(l+1)}{r^2}\left(\frac{N^2}{\omega^2}-1\right) . \tag{7.64}$$

Typically a mode is trapped between two zeros r_1 and r_2 of K, and equation (7.33) is immediately valid. Thus the frequencies are determined by

$$\int_{r_1}^{r_2} L\left(\frac{N^2}{\omega^2}-1\right)^{1/2}\frac{\mathrm{d}r}{r} = (n-1/2)\pi , \tag{7.65}$$

or

$$\int_{r_1}^{r_2} \left(\frac{N^2}{\omega^2}-1\right)^{1/2}\frac{\mathrm{d}r}{r} = \frac{(n-1/2)\pi}{L} . \tag{7.66}$$

Here the left-hand side is solely a function of ω, so that equation (7.66) can be written, in analogy with equation (7.40), as

$$\frac{n-1/2}{L} = G(\omega) , \tag{7.67}$$

where

$$G(\omega) = \frac{1}{\pi}\int_{r_1}^{r_2}\left(\frac{N^2}{\omega^2}-1\right)^{1/2}\frac{\mathrm{d}r}{r} . \tag{7.68}$$

I have here implicitly assumed that N has a single maximum, so that there is a single, well-defined trapping region at each frequency. In many stellar models, including some models of the Sun, there may be several maxima in N, and this may give rise to, at least mathematically, interesting phenomena. Roughly speaking, to each maximum there corresponds asymptotically a separate spectrum of g modes; where modes corresponding to different regions happen to have nearly the same frequencies, the modes may interact in "avoided crossings" (*e.g.* Christensen-Dalsgaard, Dziembowski & Gough 1980).

In the model illustrated in Figure 5.2 N has a weak secondary maximum near $r/R = 0.35$, and at a frequency of about $410\,\mu$Hz; this is in fact faintly reflected in the behaviour of the frequencies shown in Figure 5.6, where there is an accumulation of modes at this frequency, for $l > 15$. I neglect this local maximum and assume that N has a single maximum, $N_{\max}$, in the interior of the Sun; from equation (7.68) it then follows that

$$G(\omega) \to 0 \qquad \text{for } \omega \to N_{\max} . \tag{7.69}$$

Consequently

$$\omega \to N_{\max} \qquad \text{for } L \to \infty . \tag{7.70}$$

This behaviour is clearly visible in Figures 5.6 and 5.7.

For high-order, low-degree g modes ω is much smaller than N over most of the interval $[r_1, r_2]$. This suggests that a similar approximation to the one leading to equation (7.51) should be possible. In fact, the integral may be expanded near the centre, in much the same way as the integral in equation (7.39), by using the fact that $N \sim r$ near $r = 0$. However, the expansion near the upper turning point can apparently not be done in a similarly

simple fashion, and in any case the result does not quite have the correct dependence on l. A proper asymptotic analysis (Tassoul 1980) shows that the frequencies of low-degree, high-order g modes are given by

$$\omega = \frac{L \int_{r_1}^{r_2} N \frac{\mathrm{d}r}{r}}{\pi(n + l/2 + \alpha_\mathrm{g})} , \tag{7.71}$$

where α_g is a phase constant. Thus in this case the *periods* are asymptotically equally spaced in the order of the mode. The spacing decreases with increasing l, as is also obvious from Figure 5.6.

The analysis was carried to the next asymptotic order by Tassoul (1980). Ellis (1988), Provost & Berthomieu (1986) and Gabriel (1986) compared the resulting expressions with numerically computed frequencies for polytropic or solar models.

In the trapping region the eigenfunction is given by equation (7.34). We may assume that $\omega^2 \ll S_l^2$, and so obtain

$$\begin{aligned} \xi_r(r) &\simeq A\rho^{-1/2} r^{-1} c^{-1/2} \left(\frac{S_l}{\omega}\right)^{1/2} \left|\frac{N^2}{\omega^2} - 1\right|^{-1/4} \cos\left[L \int_{r_1}^{r} \left(\frac{N^2}{\omega^2} - 1\right)^{1/2} \frac{\mathrm{d}r'}{r'} - \frac{\pi}{4}\right] \\ &= A \left(\frac{L}{\omega}\right)^{1/2} \rho^{-1/2} r^{-3/2} \left|\frac{N^2}{\omega^2} - 1\right|^{-1/4} \cos\left[L \int_{r_1}^{r} \left(\frac{N^2}{\omega^2} - 1\right)^{1/2} \frac{\mathrm{d}r'}{r'} - \frac{\pi}{4}\right] . \end{aligned} \tag{7.72}$$

Except close to the turning points r_1, r_2 we may assume that $N^2/\omega^2 \gg 1$ (note, from Figure 5.2, that N increases very rapidly from 0 at the centre and at the base of the convection zone). Here, therefore,

$$\xi_r(r) \simeq A L^{1/2} \rho^{-1/2} r^{-3/2} N^{-1/2} \cos\left[L \int_{r_1}^{r} \left(\frac{N^2}{\omega^2} - 1\right)^{1/2} \frac{\mathrm{d}r'}{r'} - \frac{\pi}{4}\right] . \tag{7.73}$$

Hence we expect that $\rho^{1/2} r^{3/2} N^{1/2} \xi_r$ behaves like a distorted cosine function. This is confirmed by Figure 7.4. Thus equation (7.73), as the corresponding equation for the p modes, gives a fairly accurate description of the eigenfunction in the trapping region.

Outside the trapping region the eigenfunction locally decays exponentially; this is also described by saying that the mode is *evanescent*. In particular, g modes are always evanescent in convection zones. From Figure 5.2 it follows that in the solar case this evanescent region is essentially restricted to the convection zone for $\nu < 200\,\mu$Hz. At higher frequencies the evanescent region extends more deeply, and for frequencies near the maximum in N the mode is oscillatory only in a narrow region around $x = 0.1$. Thus one would expect such modes to be very efficiently trapped. To study the trapping I use the asymptotic expression (7.36). In the convection zone we can assume that $N = 0$; and for low-frequency (and high-degree) modes I neglect ω^2/S_l^2 compared with 1. Then $K \simeq -L^2/r^2$, and the variation in ξ_r through the convection zone may be approximated by

$$\begin{aligned} \xi_r(r) &\simeq \frac{1}{2} \left(\frac{L}{\omega}\right)^{1/2} \rho^{-1/2} r^{-3/2} \exp\left(-L \int_{r_2}^{r} \frac{\mathrm{d}r'}{r'}\right) \\ &= \frac{1}{2} \left(\frac{L}{\omega}\right)^{1/2} {r_2}^L \rho^{-1/2} r^{-(3/2+L)} . \end{aligned} \tag{7.74}$$

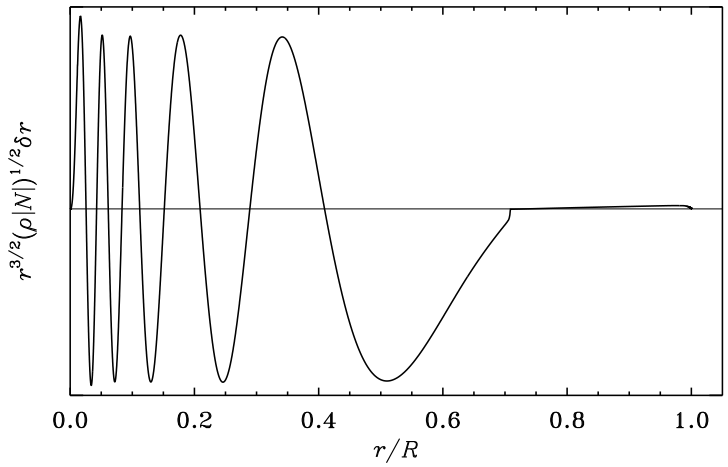

Figure 7.4: Scaled eigenfunction for high-order g mode of degree 2, radial order $n = -10$ and frequency $\nu = 104\,\mu$Hz in a normal solar model (the same mode as was shown in Figure 5.10b). According to the asymptotic equation (7.73) the quantity plotted should oscillate between fixed limits in the region where the mode is trapped.

Thus the density decrease with increasing radius causes an increase in the amplitude, but this is compensated for by the power law decrease represented by r^{-L} (note that this is the global manifestation of the locally exponential behaviour in the evanescent region). To get an idea about the relative importance of these two effects I note that the radius $r_{\rm b}$ at the base of the solar convection zone is about 0.7 R, whereas the ratio between the surface density and the density at the base of the convection zone is about 10^{-6}. Thus we obtain

$$\xi_r(r_{\rm b})/\xi_r(R) \sim 10^{-3}(0.7)^{-(3/2+L)} \sim 10^{-2.8+0.15L} \; . \tag{7.75}$$

This approximation, however, assumed the validity of the asymptotic expression (7.36) right up to the surface. This is not true, as the assumptions underlying the analysis break down close to the surface where the pressure scale height becomes small. It appears that these effects dominate unless l is quite large. An attempt at analyzing this, based on the more complete asymptotic theory to be described in the following section, is provided in Section 7.6.2.

This analysis roughly describes the trapping of low-frequency modes. At higher frequencies the deepening of the evanescent region must also be taken into account, and the asymptotic analysis becomes rather complicated. Reference may be made, however, to the numerical results presented in Figures 5.12 and 5.13. At low frequencies the increase in the interior amplitude with degree, at fixed frequency, is roughly in accordance with the asymptotic discussion given above. The steep increase with increasing frequency at $\nu > 400\,\mu$Hz is related to the faint local maximum in N at that frequency, which was discussed above (*cf.* Figure 5.2); modes with higher frequency suddenly get trapped much deeper in the

Sun, and their maximum amplitudes consequently rise very rapidly. For comparison one might note that a mode with a velocity amplitude of $1\,\mathrm{m\,sec^{-1}}$ and a period of 1 hour has a relative surface displacement amplitude of about 10^{-6}. Thus modes with an amplitude ratio of more than 10^6 are not likely to be seen. Clearly there is little hope of observing g modes of degree greater than 20.

A more careful analysis than presented here would probably allow an understanding of many of the features shown in Figures 5.12 and 5.13. This would be interesting but has, as far as I know, not been undertaken so far.

7.5 A general asymptotic expression

An approximate asymptotic description of the oscillations has been derived by Gough (see Deubner & Gough 1984), on the basis of earlier work by Lamb (1932). This does not assume that the pressure and density scale heights are much larger than the wavelength; but it assumes that the oscillations vary much more rapidly than r and g, so that the problem is locally one of oscillations of a plane-parallel layer under constant gravity. Also, as usual, the perturbation in the gravitational potential is neglected. Then the governing equations are equations (5.12) and (5.13), but without the term in $2/r$ in the former. When manipulating the equations, I neglect derivatives of r and g, but keep derivatives of the thermodynamic quantities. I note that Gough (1993) generalized this treatment to include also sphericity and varying gravity, although at the expense of obtaining considerably more complicated expressions.

7.5.1 Derivation of the asymptotic expression

The trick of the analysis is to write the equations in terms of

$$\chi = \mathrm{div}\,\boldsymbol{\delta r}\ . \tag{7.76}$$

By using the equation of continuity and the condition of adiabaticity we may also write χ as

$$\chi = -\frac{1}{\Gamma_1}\left(\frac{p'}{p} - \frac{\rho g}{p}\xi_r\right)\ . \tag{7.77}$$

The oscillation equations can be written as

$$\frac{\mathrm{d}\xi_r}{\mathrm{d}r} = \chi + \frac{1}{\rho}\frac{k_\mathrm{h}^2}{\omega^2}p'\ , \tag{7.78}$$

and

$$\frac{\mathrm{d}p'}{\mathrm{d}r} = \rho\left(\omega^2 + g\frac{\mathrm{d}\ln\rho}{\mathrm{d}r}\right)\xi_r + g\rho\chi\ . \tag{7.79}$$

In keeping with the plane-parallel approximation I have expressed l by k_h, given by equation (4.51), and I assume k_h to be constant.

By multiplying equation (7.77) by $\Gamma_1 p$ and differentiating we obtain, on using equations (7.78) and (7.79)

$$\frac{\mathrm{d}\Gamma_1}{\mathrm{d}r}p\chi - \Gamma_1 g\rho\chi + \Gamma_1 p\frac{\mathrm{d}\chi}{\mathrm{d}r} = -\rho\omega^2\xi_r + \frac{gk_\mathrm{h}^2}{\omega^2}p'\ . \tag{7.80}$$

This equation, together with equation (7.77), can be used to express ξ_r in terms of χ and its first derivative. The result is

$$\rho\left(g-\frac{\omega^4}{gk_{\rm h}^2}\right)\xi_r=\Gamma_1\left[p\chi+\frac{\omega^2}{gk_{\rm h}^2}\left(p\frac{{\rm d}\chi}{{\rm d}r}-g\rho\chi+p\frac{{\rm d}\ln\Gamma_1}{{\rm d}r}\chi\right)\right]\ . \tag{7.81}$$

Finally, by differentiating equation (7.80) and using equations (7.78), (7.79) and (7.81) to eliminate ξ_r, p' and their derivatives, we obtain the following second-order differential equation for χ:

$$\begin{aligned}&\frac{{\rm d}^2\chi}{{\rm d}r^2}+\left(\frac{2}{c^2}\frac{{\rm d}c^2}{{\rm d}r}+\frac{1}{\rho}\frac{{\rm d}\rho}{{\rm d}r}\right)\frac{{\rm d}\chi}{{\rm d}r}\\&+\left[\frac{1}{\Gamma_1}\frac{{\rm d}^2\Gamma_1}{{\rm d}r^2}-\frac{2}{\Gamma_1}\frac{{\rm d}\Gamma_1}{{\rm d}r}\frac{g\rho}{p}+k_{\rm h}^2\left(\frac{N^2}{\omega^2}-1\right)-\frac{1}{\rho}\frac{{\rm d}\rho}{{\rm d}r}\frac{1}{\Gamma_1}\frac{{\rm d}\Gamma_1}{{\rm d}r}+\frac{\rho\omega^2}{\Gamma_1 p}\right]\chi=0\ .\end{aligned} \tag{7.82}$$

Here I have introduced the adiabatic sound speed c from equation (3.52) and the buoyancy frequency N from equation (3.73).

The differential equation for χ contains no interior singular points. However, it is clear from equation (7.81) that the case where the coefficient of ξ_r vanishes is in some sense singular. This occurs when

$$\omega^2=gk_{\rm h}\ . \tag{7.83}$$

It is easy to show that then the solution for χ to equation (7.81) grows exponentially towards the interior; as this is clearly unacceptable, χ must be zero. Then equation (7.77) gives

$$p'=g\rho\xi_r\ , \tag{7.84}$$

and equation (7.78) has the solution

$$\xi_r=a\exp(k_{\rm h}r)\ , \tag{7.85}$$

where a is an arbitrary constant. It is easy to show that the resulting p' satisfies equation (7.79). Thus this is one possible solution to the plane-parallel oscillation equations. It should be noticed that equation (7.83) agrees with equation (3.84) for the frequency of a surface gravity wave. Thus the mode we have found must be identified with a surface gravity wave; and we have shown that its frequency is independent of the structure of the model below the surface, if sphericity is neglected. This result was first obtained by Gough. It is obvious from Figure 5.6 that the mode can be followed to degrees well below 10, although here the correction to the frequency given by equation (7.83) becomes significant.

To analyze equation (7.82) it is convenient to eliminate the term in ${\rm d}\chi/{\rm d}r$. Thus I introduce X by

$$X=c^2\rho^{1/2}\chi\ . \tag{7.86}$$

After considerable manipulation one then finds that X satisfies the differential equation

$$\frac{{\rm d}^2X}{{\rm d}r^2}+\left[k_{\rm h}^2\left(\frac{N^2}{\omega^2}-1\right)+\frac{\omega^2}{c^2}-\frac{1}{2}\frac{\rm d}{{\rm d}r}(H^{-1})-\frac{1}{4}H^{-2}\right]X=0\ , \tag{7.87}$$

where I have introduced the density scale height H by

$$H^{-1}=-\frac{{\rm d}\ln\rho}{{\rm d}r}\ . \tag{7.88}$$

Finally, I define a characteristic frequency ω_c by

$$\omega_c^2 = \frac{c^2}{4H^2}\left(1 - 2\frac{dH}{dr}\right) , \tag{7.89}$$

and use equation (4.60) for the acoustic frequency S_l, to obtain

$$\frac{d^2X}{dr^2} + \frac{1}{c^2}\left[S_l^2\left(\frac{N^2}{\omega^2} - 1\right) + \omega^2 - \omega_c^2\right] X = 0 . \tag{7.90}$$

This is the final second-order differential equation. Considering that the only approximations made in deriving it are the constancy of g and the neglect of the derivatives of r, it is remarkably simple.

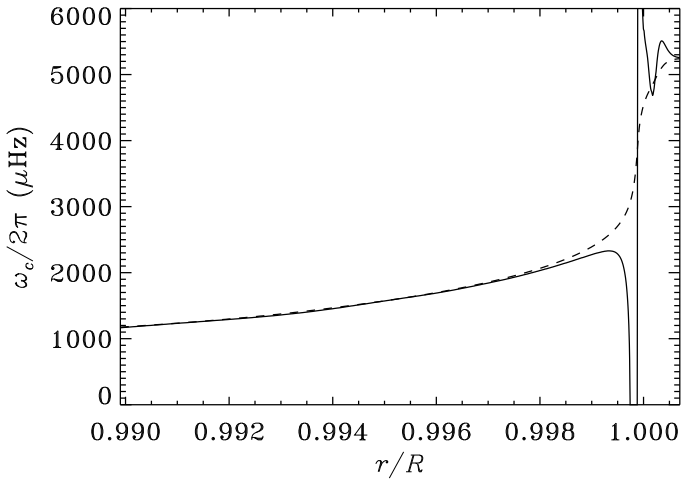

Figure 7.5: The acoustical cut-off frequency ω_c defined in equation (7.89) (solid line), and the approximation ω_a appropriate to an isothermal region [*cf.* equation (5.45); dashed line] in the outermost parts of a normal model of the present Sun.

It might be noticed that equation (7.90) can also be derived from a careful analysis of the propagation of waves in stellar interiors. This has been carried out by Gough (1986a).

Notice that if H is constant (as was assumed in Section 5.4), equation (7.89) for ω_c reduces to the frequency ω_a defined in equation (5.45). Thus ω_c, as introduced here, generalizes the acoustical cut-off frequency defined for the isothermal atmosphere. Figure 7.5 shows ω_c and ω_a in the outer parts of a normal solar model; they are in fact quite similar, except in a thin region very near the top of the convection zone, where the rapid variation in the superadiabatic gradient causes large excursions in ω_c.

Near the surface S_l^2 is small, and the coefficient of X in equation (7.90) is dominated by the last two terms; hence X is exponential when $\omega^2 < \omega_c^2$. This provides the trapping

of the modes at the surface. In the interior ω_c^2 (which roughly varies as g^2/T) is generally small, below about $600\,\mu$Hz in models of the present Sun.

We may write equation (7.90) as

$$\frac{\mathrm{d}^2X}{\mathrm{d}r^2} + K(r)X = 0 \,, \tag{7.91}$$

where

$$\begin{aligned} K(r) &= \frac{\omega^2}{c^2}\left[1 - \frac{\omega_c^2}{\omega^2} - \frac{S_l^2}{\omega^2}\left(1 - \frac{N^2}{\omega^2}\right)\right] \\ &\equiv \frac{\omega^2}{c^2}\left(1 - \frac{\omega_{l,+}^2}{\omega^2}\right)\left(1 - \frac{\omega_{l,-}^2}{\omega^2}\right) \,, \end{aligned} \tag{7.92}$$

defining the characteristic frequencies $\omega_{l,+}$ and $\omega_{l,-}$. They are plotted in Figure 7.6, in a model of the present Sun. Equation (7.92) shows that the trapping of the modes is determined by the value of the frequency, relative to behaviour of $\omega_{l,+}$ and $\omega_{l,-}$. In the interior of the Sun, particularly for large l,

$$\omega_{l,+} \simeq S_l \,; \qquad \omega_{l,-} \simeq N \,. \tag{7.93}$$

Thus here we recover the conditions for trapping discussed in Section5.2.2. This was indeed to be expected, as the assumptions entering the present formulation provide a natural transition from the previously discussed simplified asymptotic treatment to the atmospheric behaviour of the oscillations. On the other hand, near the surface where $S_l/\omega \ll 1$

$$\omega_{l,+} \simeq \omega_c \,, \tag{7.94}$$

while $\omega_{l,-}$ is small. Thus the trapping near the surface is controlled by the behaviour of $\omega_{l,+}$. As shown in Figure 7.6 trapping extends in frequency up to about 5.3 mHz, although the spike in $\omega_{l,+}$ just beneath the photosphere provides some partial reflection at even higher frequency. Also, modes with frequency $\nu \gtrsim 2\,$mHz propagate essentially to the photosphere, while modes of lower frequency are reflected at some depth in the convection zone. This behaviour is visible in the eigenfunctions shown in Figure 5.9; also it is largely responsible for the transition of the mode energy normalized with the surface displacement, shown in Figure 5.11, from steep decrease to near constancy with increasing frequency.

7.5.2 The Duvall law for p-mode frequencies

We may apply the JWKB analysis discussed in Section 7.2 to equation (7.90). Thus the asymptotic expression (7.33) for the frequency gives

$$\omega \int_{r_1}^{r_2} \left[1 - \frac{\omega_c^2}{\omega^2} - \frac{S_l^2}{\omega^2}\left(1 - \frac{N^2}{\omega^2}\right)\right]^{1/2} \frac{\mathrm{d}r}{c} \simeq \pi(n - 1/2) \,, \tag{7.95}$$

where r_1 and r_2 are adjacent zeros of K such that $K > 0$ between them.

This expression is now also formally valid for p modes. Given the rapid variation of $\omega_{l,+}$ near the surface its practical validity might be questioned. Christensen-Dalsgaard (1984c) evaluated the left-hand side of equation (7.95), substituting computed eigenfrequencies

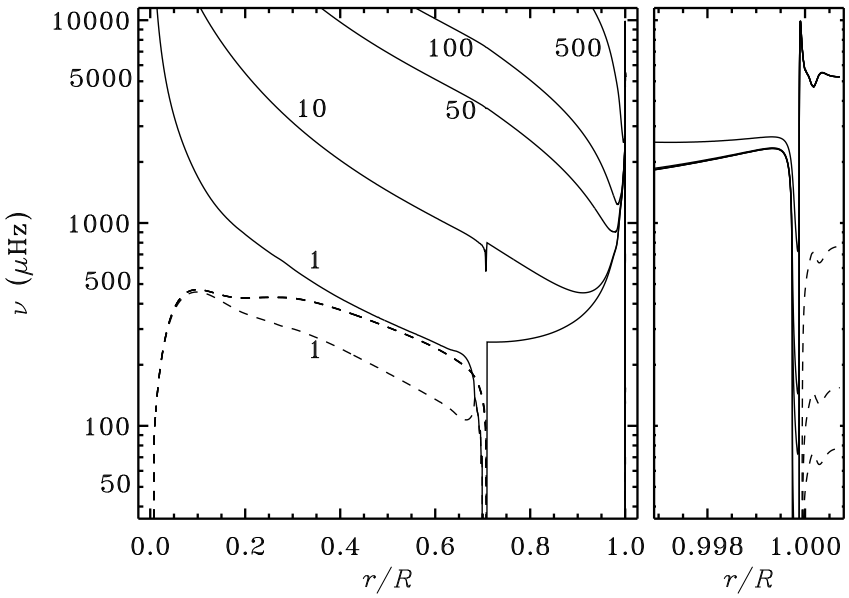

Figure 7.6: Characteristic frequencies $\omega_{l,+}/(2\pi)$ (continuous curves) and $\omega_{l,-}/(2\pi)$ (dashed curves) for a model of the present Sun (*cf.* eq. 7.92). The curves are labelled with the degree l. The right-hand panel shows the outermost parts of the model on an expanded horizontal scale. The figure may be compared with the simple characteristic frequencies plotted in Figure 5.2.

for ω, and found that the deviations from the asymptotic relation were relatively modest; however, substantially better agreement is obtained if $\omega_{\rm c}$ is replaced by the simple expression for an isothermal atmosphere, given in equation (5.45).

Equation (7.95) may be used to justify the approximate relation (7.38) for the frequencies of acoustic modes, with $\alpha = \alpha(\omega)$ being a function of frequency (see also Deubner & Gough 1984). Here I present an argument derived by Christensen-Dalsgaard & Pérez Hernández (1992). Assuming that the term in N^2 can be neglected, I write equation (7.95) as

$$\frac{\pi(n-1/2)}{\omega} \simeq F\left(\frac{\omega}{L}\right) - \frac{1}{\omega}(I_1 + I_2 + I_3) \; , \tag{7.96}$$

where

$$F(w) = \int_{r_{\rm t}}^{R} \left(1 - \frac{c^2}{w^2 r^2}\right)^{1/2} \frac{{\rm d}r}{c} \; , \tag{7.97}$$

and the dimensionless integrals $I_1 - I_3$ are defined by

$$I_1 \;=\; \omega \int_{r_2}^{R} \left(1 - \frac{S_l^2}{\omega^2}\right)^{1/2} \frac{{\rm d}r}{c} \; , \tag{7.98}$$

$$I_2 \;=\; \omega \int_{r_1}^{r_2} \left[\left(1 - \frac{S_l^2}{\omega^2}\right)^{1/2} - \left(1 - \frac{\omega_{\rm c}^2}{\omega^2} - \frac{S_l^2}{\omega^2}\right)^{1/2}\right] \frac{{\rm d}r}{c} \; , \tag{7.99}$$

$$I_3 \;=\; \omega \int_{r_\mathrm{t}}^{r_1} \left(1 - \frac{S_l^2}{\omega^2}\right)^{1/2} \frac{\mathrm{d}r}{c} \; . \tag{7.100}$$

I assume that $\omega_\mathrm{c}^2 > 0$ in the vicinity of the lower turning point, so that $r_\mathrm{t} < r_1$ [where r_t is given by equation (5.28)]; also I have assumed that $R > r_2$ for all modes of interest.

To show that equation (7.39) is approximately valid, with α being a function of ω, we must show that $I_1 + I_2 + I_3$ is predominantly a function of frequency. In so doing I make the assumptions:

- $S_l^2/\omega^2 \ll 1$ at the upper turning point.
- $\omega_\mathrm{c}^2/\omega^2 \ll 1$ at the lower turning point.

Near the upper turning point we may then neglect the term in S_l^2/ω^2, and hence the position of the turning point is approximately given by $r_2 \simeq R_\mathrm{t}$, where R_t is defined by $\omega = \omega_\mathrm{c}(R_\mathrm{t})$. Thus r_2 is a function of frequency alone; the same is therefore obviously true for I_1. I_3 is small; in fact, by expanding S_l^2 in the vicinity of r_t, neglecting the variation in ω_c and c, it is straightforward to show that

$$I_3 \simeq \frac{1}{3}\left(\frac{\omega_{\mathrm{c,t}}}{\omega}\right)^3 \omega \frac{H_{\mathrm{c,t}}}{c_\mathrm{t}} \sim \left(\frac{\omega_{\mathrm{c,t}}}{\omega}\right)^2 \; , \tag{7.101}$$

where $\omega_{\mathrm{c,t}}$, c_t and $H_{\mathrm{c,t}}$ are the values of ω_c, c and the sound-speed scale height at r_t. Thus, although I_3 depends on r_t and hence on ω/L, the term is $\mathcal{O}((\omega_\mathrm{c}/\omega)^2)$ and hence negligible.

This leaves I_2 to be dealt with. To investigate its dependence on l and ω I rewrite it as

$$I_2 = \frac{1}{\omega}\int_{r_1}^{r_2} \frac{\omega_\mathrm{c}^2}{\left(1 - \dfrac{S_l^2}{\omega^2}\right)^{1/2} + \left(1 - \dfrac{\omega_\mathrm{c}^2}{\omega^2} - \dfrac{S_l^2}{\omega^2}\right)^{1/2}} \frac{\mathrm{d}r}{c} \; . \tag{7.102}$$

Since ω_c^2/c decreases quite rapidly with increasing depth (*cf.* Figure 7.5), this integral is dominated by the region near the upper turning point r_2. It is true that the integrand is nearly singular, with an integrable singularity, at $r = r_1$; but the contribution from that is essentially $\mathcal{O}(\omega_{\mathrm{c,t}}^2/\omega^2)$ and is therefore small. Near r_2, S_l^2/ω^2 is negligible; thus we can approximate I_2 as

$$I_2 \simeq \frac{1}{\omega}\int_{r_1}^{r_2} \frac{\omega_\mathrm{c}^2}{1 + \left(1 - \dfrac{\omega_\mathrm{c}^2}{\omega^2}\right)^{1/2}} \frac{\mathrm{d}r}{c}, \tag{7.103}$$

which is obviously a function of frequency alone.

It follows that equation (7.96) may finally be written as

$$\int_{r_\mathrm{t}}^{R} \left(1 - \frac{L^2c^2}{\omega^2 r^2}\right)^{1/2} \frac{\mathrm{d}r}{c} = \frac{[n + \alpha(\omega)]\pi}{\omega} \; , \tag{7.104}$$

with

$$\alpha \simeq \alpha(\omega) = \frac{1}{\pi}(I_1 + I_2) - 1/2 \; . \tag{7.105}$$

This argument is evidently valid in general for stellar models where ω_c^2/c decreases sufficiently rapidly with increasing depth.

It is instructive to consider the analysis for the special case where the outer layers of the star can be approximated by an adiabatically stratified, plane-parallel layer; also I neglect the variation of Γ_1. Then we obtain equation (7.43) for c, and furthermore

$$\omega_c^2 = \frac{g\mu_p}{4(R-r)}\left(1+\frac{2}{\mu_p}\right) , \tag{7.106}$$

where $\mu_p = 1/(\Gamma_1 - 1)$ is the effective polytropic index of the layer. Finally N is zero. From equation (7.106) ω_c is small except near the surface, and so it is reasonable to neglect it in most of the region where the p mode is trapped (notice, however, that this becomes questionable for high l, where the trapping region is confined very close to the surface). To approximate equation (7.95) I use a trick similar to that employed to derive equation (7.51). Thus I write equation (7.95) as

$$\begin{aligned}\frac{\pi(n-1/2)}{\omega} &= \int_{r_1}^{R}\left(1-\frac{S_l^2}{\omega^2}\right)^{1/2}\frac{\mathrm{d}r}{c} - \int_{r_2}^{R}\left(1-\frac{S_l^2}{\omega^2}\right)^{1/2}\frac{\mathrm{d}r}{c} \\ &- \int_{r_1}^{r_2}\left[\left(1-\frac{S_l^2}{\omega^2}\right)^{1/2} - \left(1-\frac{\omega_c^2}{\omega^2}-\frac{S_l^2}{\omega^2}\right)^{1/2}\right]\frac{\mathrm{d}r}{c} .\end{aligned} \tag{7.107}$$

Here, approximately, r_2 is given by $\omega_c(r_2) = \omega$, and is therefore close to the surface. Furthermore, the dominant contribution to the third integral in question (7.107) comes from the region near r_2. In the last two integrals I therefore use the approximations (7.43) and (7.106) for c and ω_c; furthermore I neglect the variation of r in S_l. These integrals may then, with a little effort, be evaluated analytically. The result is

$$\frac{\pi(n-\frac{1}{2})}{\omega} = \int_{r_1}^{R}\left(1-\frac{S_l^2}{\omega^2}\right)^{1/2}\frac{\mathrm{d}r}{c} - \frac{1}{2}[\mu_p(\mu_p+2)]^{1/2}\frac{\pi}{\omega} . \tag{7.108}$$

This may also be written as equation (7.39), with

$$\alpha = 1/2[\mu_p(\mu_p+2)]^{1/2} - 1/2 . \tag{7.109}$$

Thus in this case α is a constant which is related to the effective polytropic index of the surface layers.

Exercise 7.3:

Derive equation (7.108).

If the entire layer is polytropic, with equation (7.39) and (7.106) everywhere valid, equation (7.90) may be solved analytically (*e.g.* Christensen-Dalsgaard 1980). The condition that the solution decreases exponentially at great depths determines the eigenfrequencies as

$$\omega^2 = \frac{2}{\mu_p}\left(n+\frac{\mu_p}{2}\right)L\frac{g}{R} . \tag{7.110}$$

This is in accordance with equation (7.45) obtained asymptotically, but with a different α,

$$\alpha = \frac{\mu_{\rm p}}{2} \; . \tag{7.111}$$

It is easy to show that the difference between this exact α and the asymptotic approximation in equation (7.109) is small; it tends to zero for large $\mu_{\rm p}$.

A minor point in these relations concerns the definition of L (which also enters into $S_l = cL/r$). In the analysis I have so far taken $L = \sqrt{l(l+1)}$. In fact, it may be shown from a more careful analysis of the asymptotic behaviour of the oscillation equations near the centre that a more appropriate choice would have been $L_0 = l + 1/2$ (note, however, that $L = L_0 + \mathcal{O}(l^{-1})$ and that even for $l = 1$ they are very similar). In the rest of this chapter I shall replace L by L_0 and, for convenience, suppress the subscript '0'. [Note that this was also used in the formulation of equation (7.52).]

7.6 Asymptotic properties of eigenfunctions

An initial discussion of p- and g-mode eigenfunctions was presented above, based on the simplified asymptotic description (*cf.* eqs 7.63 and 7.73). It was noted that the presence of singularities in the asymptotic equations caused problems in these approximations, particularly for the phase of the p-mode eigenfunction. Such problems are avoided in the formulation developed in Section 7.5. That formulation, on the other hand, was derived under the assumption that derivatives of r and g could be neglected. Thus, as is indeed found from numerical applications, a straightforward derivation of eigenfunctions from asymptotic analysis of (7.90) leads to amplitude functions deviating from the correct variation by low powers of r or g.

As already mentioned, a more complete asymptotic description which does not suffer from this approximation was developed by Gough (1993). In a formal sense it is quite similar to the formulation presented here, although with considerably more complicated expressions for the characteristic frequencies and eigenfunction scalings. It is likely that an asymptotic analysis based on these equations would yield the correct behaviour; however, such an analysis has apparently not been published, and will not be attempted here. Instead I shall apply a pragmatic, although certainly not rigorous, approach. The analysis in Sections 7.3 and 7.4 is correct, to leading order, away from the singular points. Consequently, we can expect that the variation of the amplitude functions in equations (7.63) and (7.73) are correct in these regions. I shall assume that this is the case and obtain the relevant powers of r and/or g in the analysis of equation (7.90) such that the final p- and g-mode expressions have the correct behaviour [the dependence with c and ρ is included fully in the derivation of equation (7.90) and is therefore correctly included]. What is gained by using equation (7.90) is therefore principally the correct treatment of the phases at the turning points.

7.6.1 Asymptotic properties of the p-mode eigenfunctions

I neglect the term in N^2 in equation (7.90), and assume that there is a region outside $r_{\rm t}$ where $\omega_{\rm c}^2$ can be neglected. In that region, except near $r_{\rm t}$, JWKB analysis of equation (7.90) leads to the following approximate solution for X:

$$X(r) \simeq A_X c^{1/2} r^{-1} \left(1 - \frac{L^2c^2}{\omega^2 r^2}\right)^{-1/4} \cos\left[\omega \int_{r_{\rm t}}^{r} \left(1 - \frac{L^2c^2}{\omega^2 r'^2}\right)^{1/2} \frac{{\rm d}r'}{c} - \frac{\pi}{4}\right] , \tag{7.112}$$

where the constant A_X is determined by the boundary conditions; the factor r^{-1} does not follow from the analysis but was, as discussed above, introduced to obtain the correct final amplitude function. An expression for ξ_r can be derived from the general equation (7.81). I neglect the derivative of Γ_1 and write the equation as

$$\rho g \left(1 - \frac{\omega^4}{\omega_{\rm f}^4}\right) \xi_r \simeq \Gamma_1 p \left[\chi + \frac{\omega^2}{g k_{\rm h}^2} \left(\frac{{\rm d}\chi}{{\rm d}r} - \frac{\Gamma_1 g}{c^2}\chi\right)\right] , \tag{7.113}$$

where $\omega_{\rm f}^2 = g k_{\rm h}$ is the squared f-mode frequency. For high-order p modes we can assume that $\omega \gg \omega_{\rm f}$. On the right-hand side we need to estimate the term in ${\rm d}\chi/{\rm d}r$, compared with the terms in χ. To do so, when differentiating here and in the following I assume that the eigenfunction varies on a scale short compared with scale heights of equilibrium quantities and only differentiate through the argument of cos in equation (7.112). It follows that the amplitude of ${\rm d}\chi/{\rm d}r$ is, to leading order, ω/c times the amplitude of χ. Consequently, the magnitudes of the coefficients to χ in the three terms in the square bracket on the right-hand side of equation (7.113) are

$$1 , \qquad \frac{\omega^3}{g c k_{\rm h}^2} , \qquad \frac{\omega^2}{k_{\rm h}^2}\frac{\Gamma_1}{c^2} . \tag{7.114}$$

To estimate the magnitude of the second component I write it as

$$\frac{\omega^2}{c^2 k_{\rm h}^2}\frac{\omega c}{g} = \frac{\omega^2}{S_l^2}\frac{\omega c}{g} . \tag{7.115}$$

In the first factor $\omega > S_l$ in regions of p-mode trapping. The second factor may be estimated from equation (5.18), neglecting ∇_μ, by writing it as

$$N^2 \simeq \frac{\Gamma_1 g^2}{c^2}(\nabla_{\rm ad} - \nabla) ; \tag{7.116}$$

thus $\omega c/g \sim (\nabla_{\rm ad} - \nabla)^{1/2}\omega/N \gg 1$ for typical p modes, at least in radiative regions where $\nabla_{\rm ad} - \nabla$ is of order unity. (Near the surface, in convective regions where this estimate is not valid, it is typically the case that $\omega^2 \gg S_l^2$.) It follows that the second component in the set (7.114) is typically much greater than unity. The ratio between the second and third components is

$$\frac{\Gamma_1 g}{\omega c} \simeq \frac{\Gamma_2^{1/2} N}{(\nabla_{\rm ad} - \nabla)^{1/2}\omega} , \tag{7.117}$$

which is again typically much smaller than unity.

Using these estimates, it follows from equations (7.113) and (7.112) that

$$\begin{aligned} \xi_r &\simeq -\frac{c^2}{\omega^2}\frac{{\rm d}\chi}{{\rm d}r} \simeq -\rho^{-1/2}\omega^{-2}\frac{{\rm d}X}{{\rm d}r} \\ &\simeq -A_X \omega^{-1}(\rho c)^{-1/2} r^{-1} \left(1 - \frac{L^2 c^2}{\omega^2 r^2}\right)^{1/4} \cos\left[\omega \int_{r_{\rm t}}^{r} \left(1 - \frac{L^2 c^2}{\omega^2 r'^2}\right)^{1/2} \frac{{\rm d}r'}{c} + \frac{\pi}{4}\right] . \end{aligned} \tag{7.118}$$

By using equation (7.104) this equation may be written as

$$\begin{aligned} &\xi_r(r) \simeq \\ &A\,(\rho c)^{-1/2} r^{-1} \left(1 - \frac{L^2 c^2}{\omega^2 r^2}\right)^{1/4} \cos\left[\omega \int_{r}^{R} \left(1 - \frac{L^2 c^2}{\omega^2 r'^2}\right)^{1/2} \frac{{\rm d}r'}{c} - (\alpha + 1/4)\pi\right] , \end{aligned} \tag{7.119}$$

where A is a new constant; this corresponds to equation (7.63).

To find the horizontal displacement I note that in equation (5.12) the first term on the right-hand side can be neglected compared with the left-hand side, so that

$$\frac{\mathrm{d}\xi_r}{\mathrm{d}r} \simeq \frac{1}{\rho c^2}\left(\frac{S_l^2}{\omega^2}-1\right)p' \simeq -\frac{r\omega^2}{c^2}\left(1-\frac{S_l^2}{\omega^2}\right)\xi_\mathrm{h}\ , \tag{7.120}$$

using equation (4.39). Thus

$$\xi_\mathrm{h}(r) \simeq -\frac{c^2}{r\omega^2}\left(1-\frac{S_l^2}{\omega^2}\right)^{-1}\frac{\mathrm{d}\xi_r}{\mathrm{d}r} \simeq \tag{7.121}$$

$$-A\,\rho^{-1/2}c^{1/2}r^{-2}\omega^{-1}\left(1-\frac{L^2c^2}{\omega^2r^2}\right)^{-1/4}\sin\left[\omega\int_r^R\left(1-\frac{L^2c^2}{\omega^2r'^2}\right)^{1/2}\frac{\mathrm{d}r'}{c}-(\alpha+1/4)\pi\right]\ .$$

It may be noted that the ratio between the amplitudes of the root-mean-square lengths of the horizontal and vertical components of the displacement is

$$\left|\frac{L\xi_\mathrm{h}}{\xi_r}\right| \sim \frac{Lc}{r\omega}\left(1-\frac{L^2c^2}{\omega^2r^2}\right)^{-1/2} = \frac{S_l}{\omega}\left(1-\frac{S_l^2}{\omega^2}\right)^{-1/2} \tag{7.122}$$

(*cf.* eq. 4.45); thus well above the lower turning point, where $\omega \gg S_l$, the oscillation is predominantly vertical.

From these expressions, we can finally find the asymptotic form of the energy integral $\mathcal{E}$ (*cf.* eq. 4.47), replacing $\sin^2$ and $\cos^2$ by the average value 1/2:

$$\begin{aligned}\mathcal{E} &\simeq 2\pi A^2\int_{r_\mathrm{t}}^R\left[c^{-1}\left(1-\frac{L^2c^2}{\omega^2r^2}\right)^{1/2}+\frac{L^2c}{\omega^2r^2}\left(1-\frac{L^2c^2}{\omega^2r^2}\right)^{-1/2}\right]\mathrm{d}r \\ &\simeq 2\pi A^2\int_{r_\mathrm{t}}^R\left(1-\frac{L^2c^2}{\omega^2r^2}\right)^{-1/2}\frac{\mathrm{d}r}{c}\ .\end{aligned} \tag{7.123}$$

7.6.2 Asymptotic properties of the g-mode eigenfunctions

We consider the region where a g mode is trapped, and assume that $\omega^2 \ll S_l^2, N^2$. Then

$$K \simeq k_\mathrm{h}^2\left(\frac{N^2}{\omega^2}-1\right)\ . \tag{7.124}$$

In the corresponding JWKB expression for the eigenfunction, comparison with equation (7.72) will show that the extra factor $gr^{-3/2}$ must be included. Thus we obtain

$$X(r) \simeq Agr^{-3/2}\left(\frac{N^2}{\omega^2}-1\right)^{-1/4}\cos\left[\int_{r_1}^r k_\mathrm{h}\left(\frac{N^2}{\omega^2}-1\right)^{1/2}\mathrm{d}r'-\frac{\pi}{4}\right]\ , \tag{7.125}$$

where $k_\mathrm{h}^{-1/2}$ was assumed to be constant and was absorbed in the amplitude A. To determine ξ_r we use again equation (7.113). On the left-hand side we can assume that $\omega \ll \omega_\mathrm{f}$. On the right-hand side, according to equation (7.125) the amplitude of $\mathrm{d}\chi/\mathrm{d}r$ is now, to

leading order, $k_{\rm h}N/\omega$ times the amplitude of χ. Thus the magnitudes of the three terms on the right-hand side of equation (7.113) scale as

$$1\ , \qquad \frac{\omega N}{g k_{\rm h}}\ , \qquad \frac{\omega^2 \Gamma_1}{k_{\rm h}^2 c^2}\ . \tag{7.126}$$

Here, using equation (7.116), the second component is

$$\frac{\omega N}{g k_{\rm h}} \simeq \frac{\omega}{c k_{\rm h}} (\nabla_{\rm ad} - \nabla)^{1/2} \simeq \frac{\omega}{S_l} (\nabla_{\rm ad} - \nabla)^{1/2} \ll 1\ , \tag{7.127}$$

and the third component is

$$\frac{\omega^2 \Gamma_1}{k_{\rm h}^2 c^2} = \Gamma_1 \frac{\omega^2}{S_l^2} \ll 1\ . \tag{7.128}$$

Thus the dominant term is the first. The result finally is

$$\begin{aligned} \xi_r &\simeq \frac{c^2}{g}\chi = \rho^{-1/2} g^{-1} X \\ &\simeq A \rho^{-1/2} r^{-3/2} \left(\frac{N^2}{\omega^2} - 1\right)^{-1/4} \cos\left[\int_{r_1}^r \frac{L}{r}\left(\frac{N^2}{\omega^2} - 1\right)^{1/2} {\rm d}r' - \frac{\pi}{4}\right]\ . \end{aligned} \tag{7.129}$$

To find the horizontal displacement we again use equation (7.120), now approximated by

$$\frac{{\rm d}\xi_r}{{\rm d}r} \simeq \frac{L^2}{r}\xi_{\rm h}\ . \tag{7.130}$$

Thus we obtain

$$\begin{aligned} \xi_{\rm h} &\simeq \frac{r}{L^2}\frac{{\rm d}\xi_r}{{\rm d}r} \\ &\simeq -A \rho^{-1/2} L^{-1} r^{-3/2} \left(\frac{N^2}{\omega^2} - 1\right)^{1/4} \sin\left[\int_{r_1}^r \frac{L}{r}\left(\frac{N^2}{\omega^2} - 1\right)^{1/2} {\rm d}r' - \frac{\pi}{4}\right]\ . \end{aligned} \tag{7.131}$$

Here the ratio between the amplitudes of the root-mean-square lengths of the horizontal and vertical components of the displacement is therefore

$$\left|\frac{L\xi_{\rm h}}{\xi_r}\right| \sim \left(\frac{N^2}{\omega^2} - 1\right)^{1/2}\ , \tag{7.132}$$

demonstrating that the oscillation is predominantly in the horizontal direction.

We may attempt to use equation (7.90) to describe the properties of g modes in an outer convection zone, *e.g.* in the solar case, to correct for the approximations discussed in connection with equation (7.75). We assume that $N^2 \simeq 0$ and $\omega^2 \ll \omega_{\rm c}^2$, so that equation (7.90) is approximated by

$$\frac{{\rm d}^2 X}{{\rm d}r^2} = \left(\frac{L^2}{r^2} + \frac{\omega_{\rm c}^2}{c^2}\right) X = \left[\frac{L^2}{r^2} + \frac{1}{4H^2}\left(1 - 2\frac{{\rm d}H}{{\rm d}r}\right)\right] X = 0\ , \tag{7.133}$$

using equation (7.89). Compared with the equation leading to equation (7.74), this differs by the inclusion of the term in $\omega_{\rm c}^2$; since the density scale height H is much smaller than

the stellar radius near the surface, there this term dominates over L^2/r^2, unless L is very large.

It is possible to carry the analysis somewhat further if we approximate the convection zone by a plane-parallel adiabatically stratified layer, and neglect the variation in Γ_1; this approximation was also used in Sections 7.3 and 7.5.2 to analyze various aspects of the Duvall law. Then $\rho = \rho_0 z^{\mu_\mathrm{p}}$, where $z = R - r$ is the depth and, as before, $\mu_\mathrm{p} = 1/(\Gamma_1 - 1)$ is the effective polytropic index. Also, we have equations (7.43) and (7.106) for c and ω_c; we write the relevant equations as

$$c^2 = \frac{g}{\mu_\mathrm{p}} z \; , \qquad \omega_\mathrm{c}^2 = \frac{g\mu_\mathrm{p}}{4z}\left(1 + \frac{2}{\mu_\mathrm{p}}\right) \; , \qquad H^{-1} = \frac{\mu_\mathrm{p}}{z} \; . \tag{7.134}$$

It follows that equation (7.133) can be written as

$$\frac{\mathrm{d}^2 X}{\mathrm{d}z^2} - \left[\frac{L^2}{R^2} + \frac{1}{4z^2}\mu_\mathrm{p}(\mu_\mathrm{p} + 2)\right] X = 0 \; , \tag{7.135}$$

where, in accordance with the assumption of a plane-parallel layer, I replaced r by R in the first term. A solution can be found to this equation in terms of modified Bessell functions. However, here I assume that L is not very large, so that the term in z^{-2} dominates. Then the regular solution to equation (7.135) is

$$X \simeq X_0 z^{1+\mu_\mathrm{p}/2} \; , \tag{7.136}$$

where X_0 is a constant. It follows from equation (7.86) that $\chi \simeq \chi_0$ is approximately constant. To determine ξ_r we use again equation (7.113), with $\omega \ll \omega_\mathrm{f}$. Obviously the term in $\mathrm{d}\chi/\mathrm{d}r$ can be neglected; however, since formally $c^2 \to 0$ at the surface both terms in χ must be included. The result is that

$$\xi_r \simeq \frac{1}{g}\left(c^2 - \frac{\Gamma_1 r^2 \omega^2}{L^2}\right)\chi_0 \; . \tag{7.137}$$

Neglecting c^2 at the surface, this shows that χ_0 is related to $\xi_r(R)$ by

$$\chi_0 \simeq -\frac{L^2 g}{\Gamma_1 R^2 \omega^2}\xi_r(R) \; . \tag{7.138}$$

Also, it follows that equation (7.75) is replaced by

$$\xi_r(r_\mathrm{b})/\xi_r(R) \simeq -\frac{r_\mathrm{b}^2}{R^2}\frac{L^2 c(r_\mathrm{b})^2}{\omega^2 R^2}\left[\frac{1}{\Gamma_1} - \frac{\omega^2}{S_l(r_\mathrm{b})^2}\right] = -\frac{r_\mathrm{b}^4}{R^4}\frac{S_l(r_\mathrm{b})^2}{\omega^2}\left[\frac{1}{\Gamma_1} - \frac{\omega^2}{S_l(r_\mathrm{b})^2}\right] \; , \tag{7.139}$$

where I neglected the variation in mass, and typically $\omega^2/S_l(r_\mathrm{b})^2 \ll 1$. I have found that numerical results, for modes of degree $l \leq 5$, in a model of the present Sun are in reasonable agreement with this relation.

To estimate the horizontal component of the displacement I again use equation (5.12) where, however, the term in ξ_r can no longer be neglected. Since we consider an adiabatically stratified convection zone, $\Gamma^{-1}H_p^{-1} = H^{-1}$, and hence equation (5.12) can be approximated by

$$\frac{\mathrm{d}\xi_r}{\mathrm{d}r} - H^{-1}\xi_r = \frac{r\omega^2}{c^2}\left(\frac{S_l^2}{\omega^2} - 1\right)\xi_\mathrm{h} \; . \tag{7.140}$$

When differentiating ξ_r, as given by equation (7.137), we neglect derivatives of g and r; using also equations (7.134) we obtain

$$\frac{\mathrm{d}\xi_r}{\mathrm{d}r} - H^{-1}\xi_r = -\left(1 + \frac{1}{\mu_\mathrm{p}} - \frac{\Gamma_1 r^2\omega^2\mu_\mathrm{p}}{L^2 gz}\right)\chi_0 = -\Gamma_1\left(1 - \frac{\omega^2}{S_l^2}\right)\chi_0 \; ; \tag{7.141}$$

Thus equation (7.140) gives, using also equation (7.138), that

$$\xi_\mathrm{h} \simeq -\frac{\Gamma_1 c^2}{rS_l^2}\chi_0 \simeq \frac{g}{r\omega^2}\xi_r(R) \simeq \sigma^{-2}\xi(R) \tag{7.142}$$

is approximately constant in the convection zone. It should also be noticed that this result, reassuringly, is consistent with the surface condition given in equation (4.69).

It would be interesting to match this behaviour in the convection zone to the region of trapping in the interior, to obtain the asymptotic behaviour of the mode energy. However, I have so far not been able to carry this analysis through to a result which resembles the numerical behaviour.

7.7 Analysis of the Duvall law

It was shown in Section 7.5.2, on the basis of the asymptotic theory of p modes, that such modes satisfy the *Duvall law*: we can find a function $\alpha(\omega)$ of frequency such that the quantity $[n + \alpha(\omega)]/\omega$ depends principally on frequency ω and degree l only in the combination $w \equiv \omega/L$, *i.e.*,

$$\frac{(n+\alpha)\pi}{\omega} = F\left(\frac{\omega}{L}\right) \; . \tag{7.143}$$

Here the function $F(\omega/L)$ is related to the adiabatic sound speed $c(r)$ by

$$F(w) = \int_{\ln r_\mathrm{t}(w)}^{\ln R} \left(1 - \frac{a^2}{w^2}\right)^{1/2} a^{-1}\mathrm{d}\ln r \; , \tag{7.144}$$

where $a = c/r$. Also, the function $\alpha(\omega)$ is primarily determined by conditions near the stellar surface. As illustrated in Figure 7.1 the observed frequencies of solar oscillation satisfy a relation of the form given in equation (7.143) quite accurately. This suggests that these relations are useful tools for analysing solar oscillation frequencies. It should be noted, however, that they are only approximately valid. In fact, a much more precise fit to the observed frequencies can be obtained by including additional terms (*e.g.* Gough & Vorontsov 1995) which take into account the effect of the perturbation in the gravitational potential (significant at low degree) and the dependence of the modes on degree near the upper turning point (important at high degree).

In this section I illustrate some properties of the Duvall law by applying it to frequencies computed for solar models, as well as to observed frequencies. The results are based on computations by Christensen-Dalsgaard, Proffitt & Thompson (1993) who considered both normal solar models and models which included effects of diffusion and gravitational settling of helium; recent opacity tables (Iglesias, Rogers & Wilson 1992) and a reasonable approximation to the equation of state were used. Thus the results illustrate both how well modern solar models fit the observed frequencies and the sensitivity of such analyses to relatively subtle features of the model calculations, such as gravitational settling.

7.7.1 The differential form of the Duvall law

A very powerful relation can be obtained by considering the effect on equation (7.104) of small changes to the equilibrium structure. I consider two cases (two solar models or a solar model and the Sun) with the same surface radius, labelled with the superscripts $^{(1)}$ and $^{(2)}$, and introduce the differences $\delta\omega_{nl} = \omega_{nl}^{(2)} - \omega_{nl}^{(1)}$, $\delta_r c(r) = c^{(2)}(r) - c^{(1)}(r)$ and $\delta\alpha(\omega) = \alpha^{(2)}(\omega) - \alpha^{(1)}(\omega)$. By substituting $c^{(2)}(r) = c^{(1)}(r) + \delta_r c(r)$ and $\alpha^{(2)}(\omega) = \alpha^{(1)}(\omega) + \delta\alpha(\omega)$ into equation (7.104), retaining only terms linear in $\delta_r c$, $\delta\alpha$ and $\delta\omega$, one obtains

$$S_{nl}\frac{\delta\omega_{nl}}{\omega_{nl}} \simeq \int_{r_t}^{R}\left(1 - \frac{c^2L^2}{\omega_{nl}^2 r^2}\right)^{-1/2}\frac{\delta_r c}{c}\frac{\mathrm{d}r}{c} + \pi\frac{\delta\alpha(\omega_{nl})}{\omega_{nl}} , \tag{7.145}$$

where

$$S_{nl} = \int_{r_t}^{R}\left(1 - \frac{L^2c^2}{r^2\omega_{nl}^2}\right)^{-1/2}\frac{\mathrm{d}r}{c} - \pi\frac{\mathrm{d}\alpha}{\mathrm{d}\omega} , \tag{7.146}$$

and I have suppressed the superscript $^{(1)}$. This relation was first obtained by Christensen-Dalsgaard, Gough & Pérez Hernández (1988).

Exercise 7.4:

Derive equation (7.145). If initially you obtain a different result, you may be in good company: so did the referee of Christensen-Dalsgaard *et al.* (1988).

Equation (7.145) may be written as

$$S_{nl}\frac{\delta\omega_{nl}}{\omega_{nl}} \simeq \mathcal{H}_1\left(\frac{\omega_{nl}}{L}\right) + \mathcal{H}_2(\omega_{nl}) , \tag{7.147}$$

where

$$\mathcal{H}_1(w) = \int_{r_t}^{R}\left(1 - \frac{c^2}{r^2w^2}\right)^{-1/2}\frac{\delta_r c}{c}\frac{\mathrm{d}r}{c} , \tag{7.148}$$

and

$$\mathcal{H}_2(\omega) = \frac{\pi}{\omega}\delta\alpha(\omega) . \tag{7.149}$$

Some properties of this equation were discussed by Christensen-Dalsgaard, Gough & Pérez Hernández (1988) and by Christensen-Dalsgaard *et al.* (1989). As pointed out in the latter paper, $\mathcal{H}_1(\omega/L)$ and $\mathcal{H}_2(\omega)$ can be obtained separately, to within a constant, by means of a double-spline fit of the expression (7.147) to p-mode frequency differences. The dependence of $\mathcal{H}_1$ on ω/L is determined by the sound-speed difference throughout the star, whereas $\mathcal{H}_2(\omega)$ depends on differences in the upper layers of the models.

There is a close analogy between equation (7.147) and the 'exact' equation (5.90). From equations (7.123) and (7.146) it follows that S_{nl}, apart from the term in the derivative of α, is proportional to the energy integral $\mathcal{E}$. Thus one finds that the scaling Q_{nl} in equation (5.90) is essentially asymptotically equal to S_{nl}/S_0, where $S_0 = \lim_{w\to 0} S(w)$ (Christensen-Dalsgaard 1991b); one may show that $S_0 = \tau_0$ where

$$\tau_0 = \int_0^R \frac{\mathrm{d}r}{c} \tag{7.150}$$

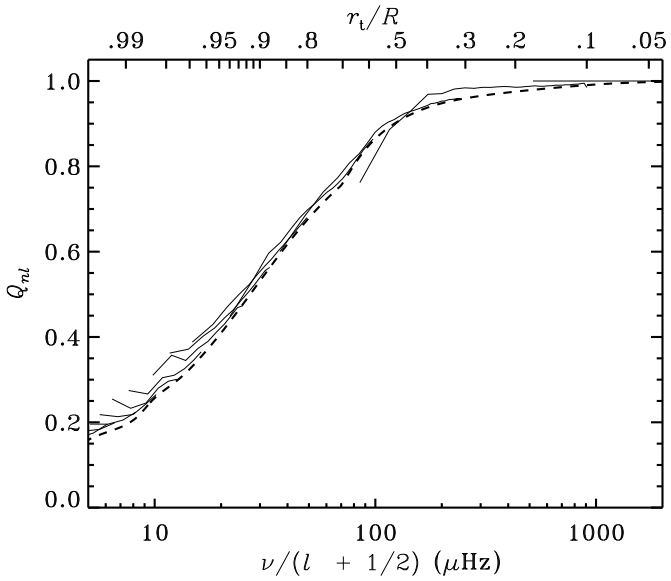

Figure 7.7: The solid lines show the inertia ratio Q_{nl}, defined in equation (5.88), against $\nu/(l+1/2)$ in a normal solar model, each curve corresponding to a given degree l. The upper abscissa shows the turning-point radius r_t, related to $\nu/(l+1/2)$ through equation (5.28). The heavy dashed curve shows the asymptotic scaling $\tilde{S}_{nl}/\tau_0$, where $\tilde{S}_{nl}$ is defined as in equation (7.146) but neglecting the term in $\mathrm{d}\alpha/\mathrm{d}\omega$.

is the acoustical radius of the star. The close correspondence between Q_{nl} and S_{nl}/τ_0 is illustrated in Figure 7.7. Furthermore, the term $\mathcal{G}(\omega)$ in equation (5.90) to some extent corresponds to the term $\mathcal{H}_2(\omega)$ in equation (7.147), in that both terms contain contributions from the uncertain regions very near the stellar surface. However, as discussed in Section 7.7.3 below $\mathcal{H}_2$ may also be used to gain information about somewhat deeper regions.

Since c/r decreases quite rapidly with increasing r, $(Lc/r\omega)^2 \ll 1$ except near the turning point r_t; hence as a rough approximation $1 - L^2c^2/r^2\omega^2$ may be replaced by 1 in the integrals in equations (7.145) and (7.146). If furthermore the terms in $\delta\alpha$ and $\mathrm{d}\alpha/\mathrm{d}\omega$ can be neglected, the result is the very simple relation between the changes in sound speed and frequency:

$$\frac{\delta\omega}{\omega} \simeq \frac{\displaystyle\int_{r_t}^{R} \frac{\delta_r c}{c}\frac{\mathrm{d}r}{c}}{\displaystyle\int_{r_t}^{R} \frac{\mathrm{d}r}{c}} \,. \tag{7.151}$$

This shows that the change in sound speed in a region of the Sun affects the frequency

with a weight determined by the time spent by the mode, regarded as a superposition of traveling waves, in that region. Thus changes near the surface, where the sound speed is low, have relatively large effects on the frequencies. Although this expression is only a rough approximation, it is a useful guide in attempts to interpret frequency differences between models, or between observed and computed frequencies.

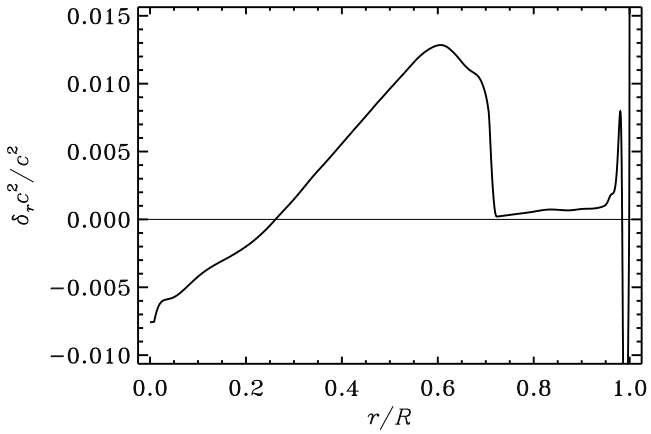

Figure 7.8: Fractional difference in sound speed between a model of the present Sun with diffusion and a normal model, without diffusion. From Christensen-Dalsgaard, Proffitt & Thompson (1993).

To illustrate the behaviour of the separation in equation (7.147) I consider differences between two models of Christensen-Dalsgaard *et al.* (1993): a model with diffusion and settling and a normal solar model. Figure 7.8 shows the sound-speed difference between these models. It is dominated by the fact that the convection zone is slightly deeper in the model with diffusion: since the temperature and sound-speed gradients are steeper in the convection zone than in the radiative region below, there is a region where the sound speed increases more rapidly with depth in the diffusive model, and this leads to the behaviour seen in the figure. Furthermore, due to settling of helium out of the convection zone the hydrogen abundance X_e in the convective envelope is higher by about 0.03 in the diffusive model, compared with the normal model. This causes differences in Γ_1, and hence in the sound speed, in the ionization zones of hydrogen and helium.

Figure 7.9a shows scaled frequency differences, at selected values of l, between these two models, plotted against ν/L (with $L = l + 1/2$; see above). I have normalized the scaling by S_0, such that it tends to unity at low degree; hence the scaled frequency differences correspond in magnitude to the differences for low-degree modes. The upper abscissa shows the location of the lower turning point, which is related to ω/L through equation (5.28). The general behaviour of the frequency differences reflects the asymptotic expression (7.147). The dependence of $S\delta\nu/\nu$ on ν/L can be understood from the sound-speed difference shown in Figure 7.8: for $\nu/L \lesssim 100\,\mu$Hz the modes are entirely trapped in the convection zone, and the frequency difference is dominated by the term $\mathcal{H}_2(\nu)$ arising from differences near

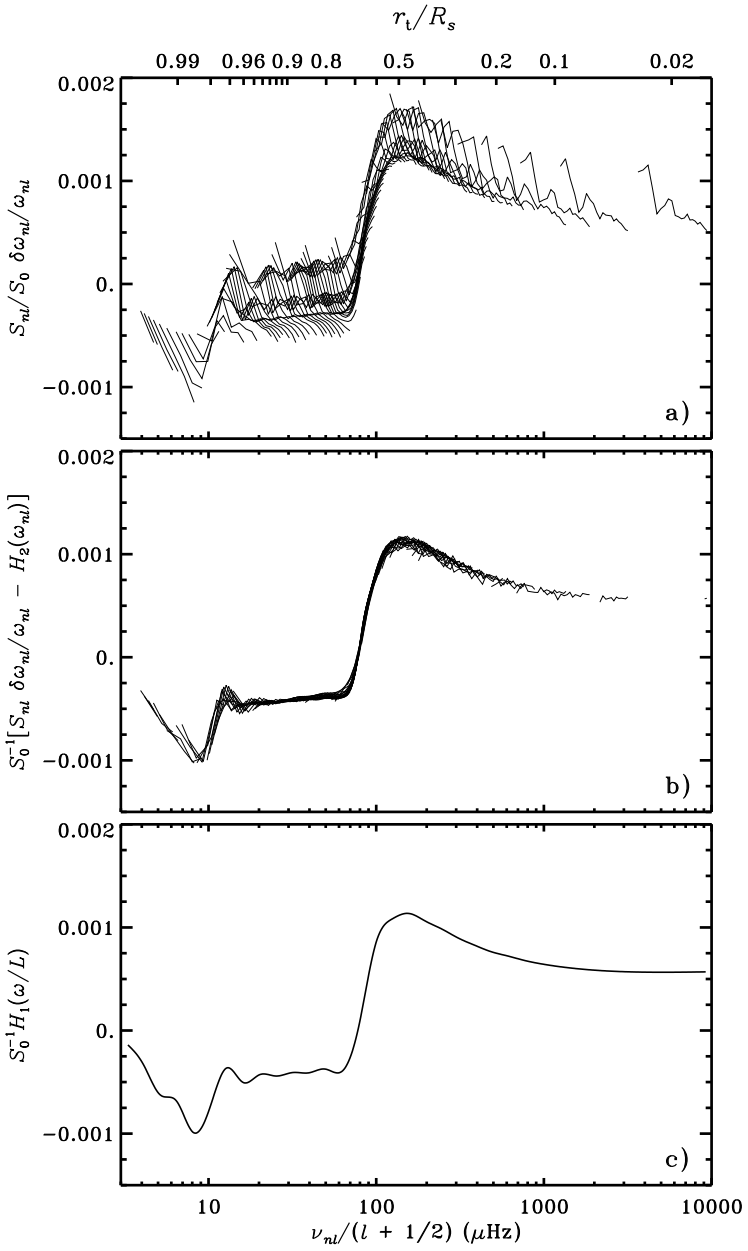

Figure 7.9: Scaled frequency differences corresponding to the model differences shown in Figure 7.8, plotted against $\nu/(l + 1/2)$. The upper abscissa shows the location of the lower turning point, which is related to $\nu/(l+1/2)$ through equation (5.28). In panels (a) and (b) points corresponding to fixed l have been connected. (a) Original scaled frequency differences. (b) Scaled differences, after subtraction of the function $\mathcal{H}_2(\omega)$ obtained from the spline fit. (c) The fitted function $\mathcal{H}_1(\omega/L)$.

the surface, particularly the difference in X_e. In contrast, modes with $\nu/L > 100\,\mu$Hz sense the substantial positive $\delta_r c$ just beneath the convection zone, and hence display a positive frequency difference; the transition occurs quite abruptly as the modes begin to penetrate beyond the convection zone.

This qualitative description suggests that the frequency differences may be analyzed in detail in terms of equation (7.147). To do so, I have determined the functions $\mathcal{H}_1$ and $\mathcal{H}_2$ by means of the spline fit of Christensen-Dalsgaard *et al.* (1989), where details about the fitting method may be found. Briefly, the procedure is to approximate $\mathcal{H}_1(\omega/L)$ and $\mathcal{H}_2(\omega)$ by splines, the coefficients of which are determined through a least-squares fit to the scaled frequency differences. The knots of the splines in $w \equiv \omega/L$ are distributed uniformly in $\log w$ over the range considered, whereas the knots for the ω-splines are uniform in ω. I used 28 knots in w and 20 knots in ω. [As a technical point, I note that in the separation in equation (7.147) $\mathcal{H}_1$ and $\mathcal{H}_2$ are evidently each only determined up to a constant term; hence in the following, when comparing $\mathcal{H}_2$ for different cases, we are permitted to shift $\mathcal{H}_2$ by a constant.]

Figure 7.9b shows the result of subtracting the function $\mathcal{H}_2(\omega)$ so obtained from the scaled frequency differences. It is evident that what remains is in fact very nearly a function of ω/L alone, directly reflecting the behaviour of $\delta_r c/c$, as discussed above. The function $\mathcal{H}_1(w)$ obtained from the fit is shown in Figure 7.9c. Similarly, Figure 7.10a shows the residual scaled frequency differences after subtraction of the term in $\mathcal{H}_1(\omega/L)$; these are clearly predominantly functions of frequency, although with some scatter. The fitted function $\mathcal{H}_2(\omega)$ is shown in Figure 7.10b.

The same analysis can obviously be applied to differences between observed frequencies and those of suitable reference models. To illustrate the power of helioseismic analysis to investigate even quite subtle features in the Sun, I consider two such reference models: one which does not include effects of settling and diffusion, and a second where settling and diffusion of helium and heavy elements are taken into account. Further details of the models were given by Christensen-Dalsgaard (1996b). The computed frequencies are compared with a set of observed data, combining modes with $l \leq 3$ from the BiSON network (Elsworth *et al.* 1994) with data for $l \geq 4$ from Libbrecht, Woodard & Kaufman (1990).

Figure 7.11a shows scaled differences between the observations and the model without diffusion and settling. It is evident already from this raw difference plot that in this case the term in $\mathcal{H}_2$ plays an important rôle. That should not be a surprise: as mentioned in Section 5.1.2 there are substantial uncertainties in the treatment of the near-surface layers and these are expected to produce effects that, when scaled, are mainly functions of frequency (see also Section 5.5.3). However, there is also evidence for a contribution from $\mathcal{H}_1$. This becomes clear if the spline fit is carried out and the contribution from $\mathcal{H}_2$ is subtracted from the scaled differences. The result is shown in Figure 7.11b, while the fitted $\mathcal{H}_1$ is shown in Figure 7.11c. There is again a sharp step corresponding in position to $r_t \simeq 0.7R$, *i.e.*, the base of the convection zone. As discussed in connection with the model comparison this may be taken as evidence that the convection zone in the Sun is somewhat deeper than in the model.

Corresponding results for the model including settling and diffusion are shown in Figure 7.12. In the original scaled differences shown in panel (a) it is difficult to discern any trend beyond the very obvious effect of the near-surface errors. Nonetheless, after carrying out the spline fit the residuals in panel (b) show a very definite dependence on ν/L, indicating remaining problems in the interior of the model. This is also clear from panel (c), which

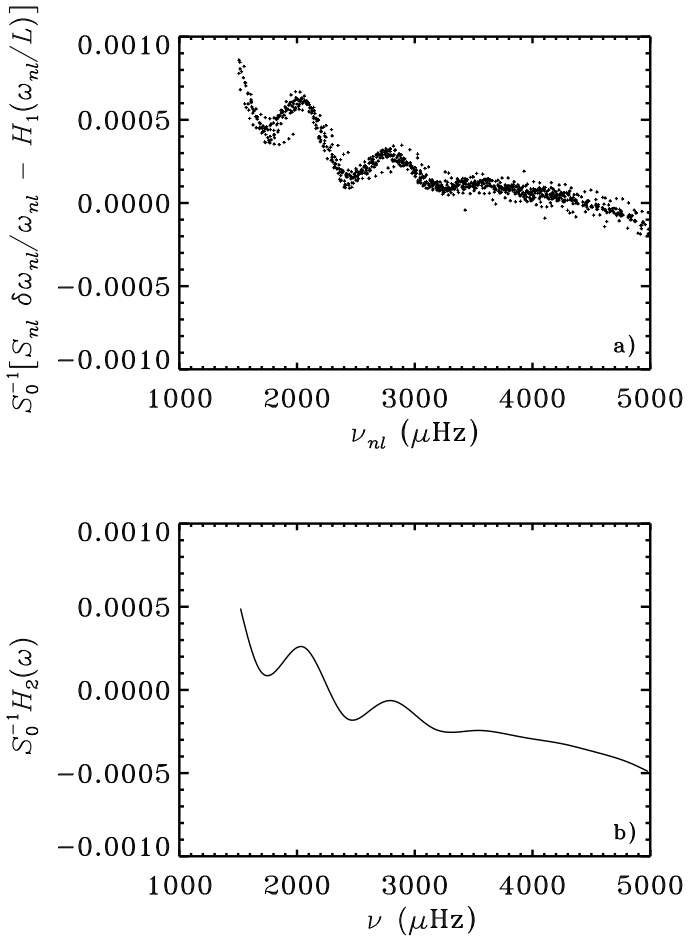

Figure 7.10: The frequency-dependent part of the scaled frequency differences corresponding to the model differences shown in Figure 7.8. (a) Scaled differences after subtraction of the function $\mathcal{H}_1(\omega/L)$ resulting from the spline fit. (b) The fitted function $\mathcal{H}_2(\omega)$.

shows the fitted function $\mathcal{H}_1$; here there is evidently a step at a turning-point location corresponding approximately to the base of the convection zone. Nevertheless, it is evident even from this simple analysis that the inclusion of diffusion and settling very substantially improves the agreement between the model and the Sun.

It is evident that there is considerably more scatter in Figure 7.11b than in the corresponding Figure 7.9b. This is due to observational errors, both random and systematic. In particular, it may be noticed that there is an apparent break at around $\nu/L \simeq 15\,\mu$Hz. In fact, the observed frequencies were obtained from two separate sets of observations, the merge taking place at $l = 400$; it has later been found that there were slight systematic errors in the high-degree set. This difficulty is clearly reflected in the fitted $\mathcal{H}_1(\omega/L)$ in Figure 7.11c. Furthermore, there appear to be problems at low degree, corresponding to

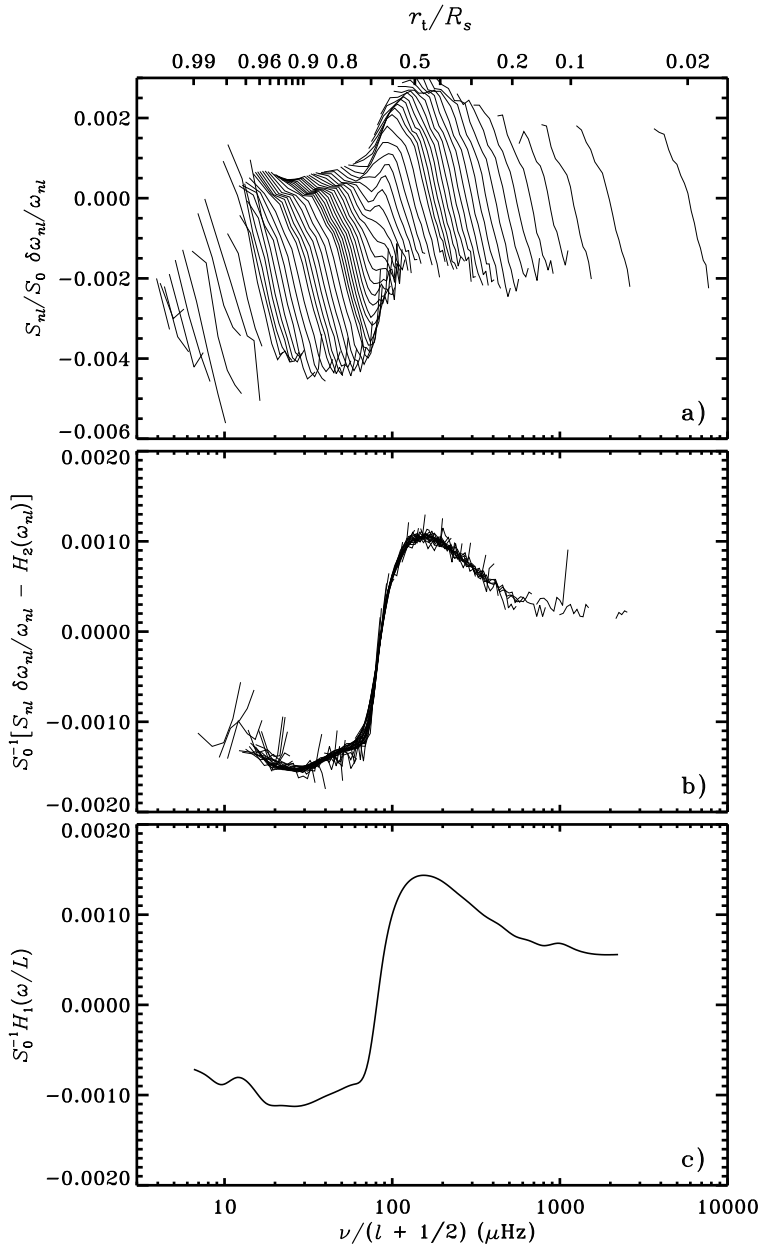

Figure 7.11: Scaled frequency differences between observed frequencies (see text) and a solar model neglecting settling and diffusion, in the sense (observations) – (model), plotted against $\nu/(l+1/2)$. The upper abscissa shows the location of the lower turning point, which is related to $\nu/(l+1/2)$ through equation (5.28). In panels (a) and (b) points corresponding to fixed l have been connected. (a) Original asymptotically scaled frequency differences. (b) Scaled differences, after subtraction of the function $\mathcal{H}_2(\omega)$ obtained from the spline fit. (c) The fitted function $\mathcal{H}_1(\omega/L)$.

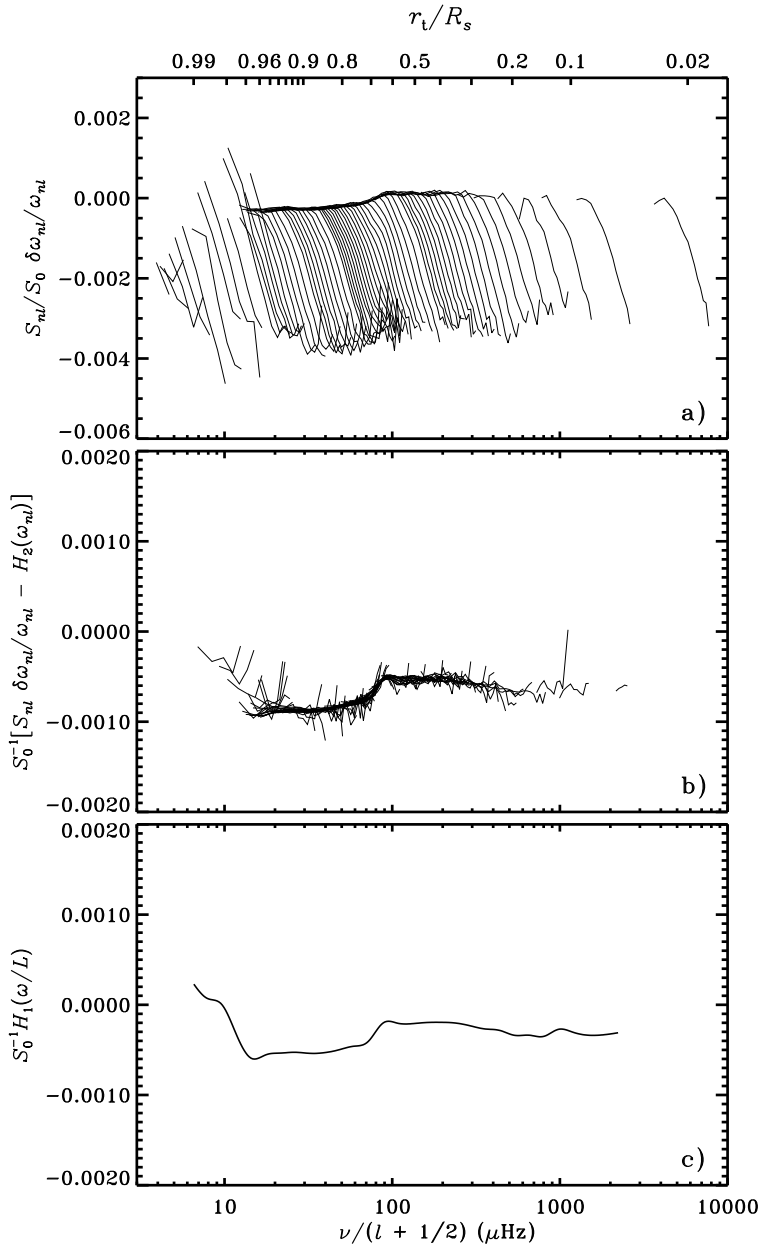

Figure 7.12: Scaled frequency differences between observed frequencies (see text) and a solar model including settling and diffusion, in the sense (observations) – (model), plotted against $\nu/(l + 1/2)$. See caption to Figure 7.11.

the highest values of ν/L.

The residual after subtraction of the fitted $\mathcal{H}_1$ from the scaled differences, and the fitted $\mathcal{H}_2$, are shown in Figure 7.13. In panel (a) are shown the residuals for the model neglecting diffusion and settling. As before, these are indeed predominantly a function of frequency.

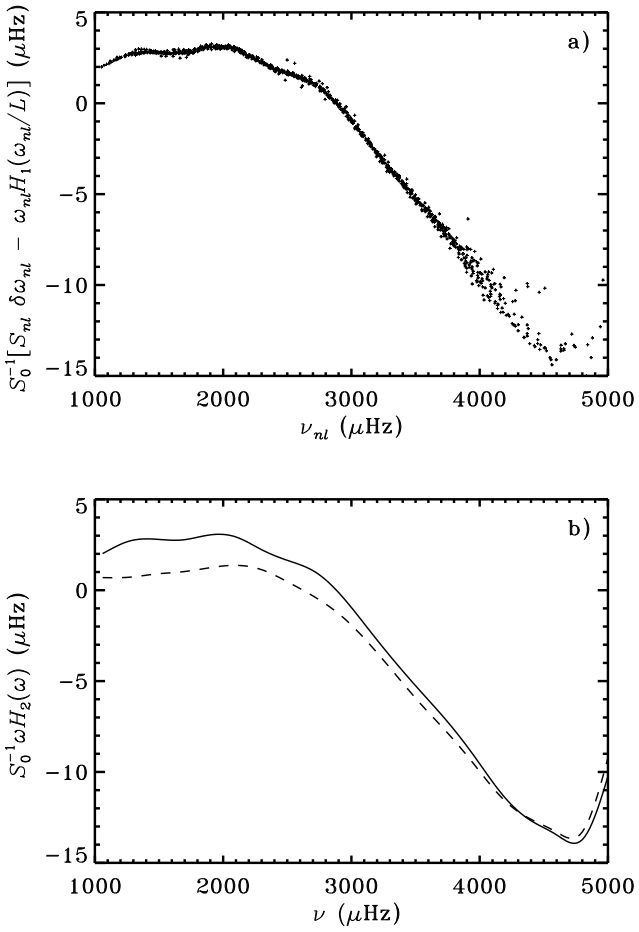

Figure 7.13: The frequency-dependent part of the scaled frequency differences between observations and models. (a) Scaled differences, shown in Figure 7.11a, after subtraction of the function $\mathcal{H}_1(\omega/L)$ resulting from the spline fit. (b) The solid line shows the fitted function $\mathcal{H}_2(\omega)$ for this data set, while the dashed line shows the corresponding fitted function obtained from the differences in Figure 7.12a.

They are dominated by a slowly varying trend which, as argued in Section 7.7.3 below reflects errors in the near-surface region of the model. However, there is also a weak but clearly noticeable oscillatory signal. As discussed in Section 7.7.3 this probably reflects a difference between the Sun and the model in the hydrogen abundance in the convective envelope. This oscillatory behaviour is also very evident in the fitted $\mathcal{H}_2(\omega)$, shown as a solid line in panel (b). In contrast, $\mathcal{H}_2(\omega)$ for the model with settling and diffusion, shown as a dashed line, gives very little evidence for such oscillations, indicating that the envelope hydrogen abundance for this model is quite similar to that of the Sun.

7.7.2 Inversion of the Duvall law

The function $F(w)$ in equation (7.143) can be determined from the observations (*cf.* Figure 7.1). Given F, equation (7.144) is an integral equation of the Abel type, and can be inverted analytically to obtain the sound speed implicitly, thus:

$$r = R\exp\left[-\frac{2}{\pi}\int_{a_\mathrm{s}}^{a}\left(w^{-2}-a^{-2}\right)^{-1/2}\frac{\mathrm{d}F}{\mathrm{d}w}\mathrm{d}w\right] \tag{7.152}$$

(Gough 1984). This relation was used by Christensen-Dalsgaard *et al.* (1985) to infer the sound speed in the solar interior. The properties of this inversion technique were discussed in considerable detail by Gough (1986b).

Exercise 7.5:

Confirm that equation (7.152) is a solution to equation (7.144). This is most simply done by substituting equation (7.144) into equation (7.152).

The asymptotic description leading to equation (7.152) clearly suffers from systematic errors. It has been found, for example, that for the most deeply penetrating modes of low degree the perturbation to the gravitational potential has a substantial effect on the functions $F(\omega/L)$ obtained by fitting the relation (7.143) to computed or observed frequencies; this may cause problems for the inversion in the solar core. Also, for modes trapped near the surface the behaviour near the upper turning point depends on the degree; this introduces what is effectively an l-dependent term in α. It is possible to generalize equation (7.143) to take such effects into account and hence obtain a substantially more precise inversion (*e.g.* Vorontsov & Shibahashi 1991).

Alternatively, it appears that the systematic errors cancel to some extent when differences are taken between inversions of different sets of frequencies. Christensen-Dalsgaard *et al.* (1985) made use of this by considering differences between inversions done for the solar data and for frequencies for a reference model. A more systematic approach follows from the separation of scaled frequency differences in equation (7.147). Here the function $\mathcal{H}_1(\omega/L)$ is related to the sound-speed difference between the models, or between the Sun and the model, through equation (7.148). As shown by Christensen-Dalsgaard, Gough & Thompson (1989), given a determination of $\mathcal{H}_1$, that equation is an integral equation for $\delta_r c/c$, with the solution

$$\frac{\delta_r c}{c} = -\frac{2a}{\pi}\frac{\mathrm{d}}{\mathrm{d}\ln r}\int_{a_\mathrm{s}}^{a}(a^2-w^2)^{-1/2}\mathcal{H}_1(w)\mathrm{d}w\,, \tag{7.153}$$

where $a_\mathrm{s} = a(R)$. [It should be noticed that the right-hand side of equation (7.148) is the same functional of w as that which arises in the asymptotic expression for the linear frequency splitting due to latitudinally-independent rotation at a rate $\Omega(r)$, with $\delta_r c/c$ instead of Ω (Gough 1984). Thus it can be inverted in the same way.]

Christensen-Dalsgaard *et al.* (1989) carried out a careful test of the differential method, as applied to several different pairs of models. Also, Christensen-Dalsgaard, Gough & Thompson (1988) used the method to invert differences between observed frequencies and frequencies computed for a solar model. Here I illustrate its properties by applying it to the

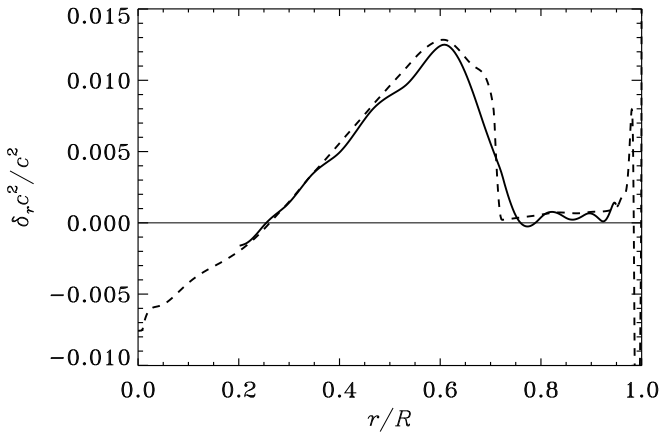

Figure 7.14: The solid line shows the difference in squared sound speed $\delta_r c^2/c^2$ inferred by applying equation (7.153) to the function $\mathcal{H}_1(\omega/L)$ shown in Figure 7.9c. For comparison, the dashed line shows the true difference between the two models. Adapted from Christensen-Dalsgaard, Proffitt & Thompson (1993).

model pair shown in Figure 7.8 and to differences between solar and computed frequencies such as those shown in Figures 7.11 and 7.12.

Figure 7.14 shows the $\delta_r c^2/c^2$ inferred from the scaled frequency differences in Figure 7.9 between the diffusive and the normal solar model, by applying equation (7.153) to the fitted function $\mathcal{H}_1(\omega/L)$ shown in Figure 7.9c. For comparison, the figure also shows the true sound-speed difference, previously plotted in Figure 7.8. It is evident that the inversion reproduces the main features of the true $\delta_r c^2/c^2$ with considerable precision. One noticeable difference is that the transition at the base of the convection zone is less sharp: as discussed in Section 9.1 it is a general property of inverse analyses that they smooth the properties of the true structure. However, otherwise the inferred and the true $\delta_r c^2/c^2$ are quite close over the entire range, $0.2R < r < 0.95R$, where the solution is plotted. At smaller and larger radii the systematic errors associated with the asymptotic representation increasingly affect the results; hence here the solution has not been obtained.

From the frequency differences illustrated in Figures 7.11 and 7.12 we may now infer the error in the sound speed in the solar models. Figure 7.15 shows the results of evaluating $\delta_r c/c$ by applying equation (7.153) to the $\mathcal{H}_1(\omega/L)$ shown in Figures 7.11c and 7.12c. The sound-speed differences are small, corresponding to errors in T/μ in the models of generally less than 2 per cent. Nonetheless, the differences are clearly highly systematic. It is interesting that the relatively subtle, and often neglected, effect of gravitational settling leads to a substantial improvement in the agreement between the model and the observations, largely by increasing the depth of the convection zone in the model. This is a striking illustration of the power of helioseismology to probe the details of the solar interior. However, it should also be pointed out that modest modifications in the opacity, well within the

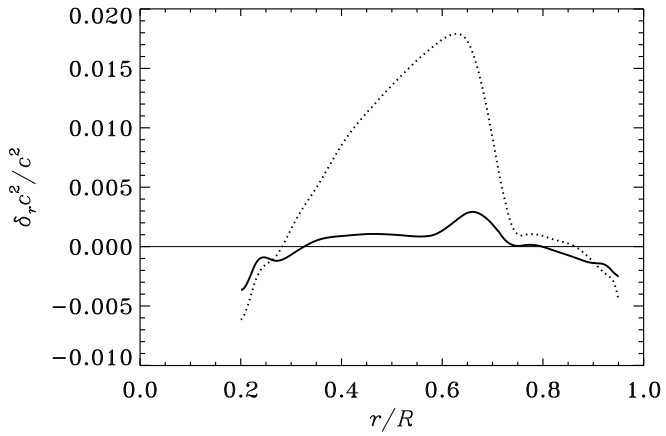

Figure 7.15: The dotted line shows the difference in squared sound speed $\delta_r c^2/c^2$ between the Sun and a solar model without diffusion and settling, inferred by applying equation (7.153) to the function $\mathcal{H}_1(\omega/L)$ shown in Figure 7.11c, corresponding to differences between observed and model frequencies. The solid line shows the corresponding $\delta_r c^2/c^2$ between the Sun and a model including diffusion and gravitational settling, obtained from $\mathcal{H}_1(\omega/L)$ in Figure 7.12c.

precision of current opacity tables, might introduce changes in the sound speed of similar magnitude. The separation of opacity uncertainties from effects of diffusion and settling is a major challenge, which will undoubtedly require better physical understanding of the processes involved.

The cause of the dominant difference between the Sun and the nondiffusive model is probably that the depth of the convection zone in the model is too small. In fact, the model with diffusion has a slightly deeper convection zone. From a more careful analysis of such results of inversions it is possible to obtain an estimate of the convection-zone depth $d_{\rm b}$ which is largely independent of other uncertainties in the model. In this way Christensen-Dalsgaard, Gough & Thompson (1991) found that $d_{\rm b} = (0.713 \pm 0.003)\, R$.

It should finally be mentioned that several other techniques have been developed to invert the Duvall law (7.143) (Brodsky & Vorontsov 1987, 1988a; Shibahashi 1988; Shibahashi & Sekii 1989). Gough & Thompson (1991) have made a comparison of these different techniques. The results suggest that, at least for the cases considered, the differential technique described here is superior. Nonasymptotic inversion of similar data sets will be discussed in Section 9.2.

7.7.3 The phase-function difference $\mathcal{H}_2(\omega)$

The function $\mathcal{H}_2(\omega)$ is predominantly determined by the region near the stellar surface. Christensen-Dalsgaard & Pérez Hernández (1992) analyzed the relation of $\mathcal{H}_2(\omega)$ to the differences in sound speed and Γ_1 in the outer parts of the Sun: differences localized very

near the surface give rise to a component of $\mathcal{H}_2$ that varies slowly with ω, whereas differences at somewhat greater depth introduce an oscillatory variation with ω in $\mathcal{H}_2$, the "frequency" of which increases with the depth of the difference. This is in fact a general property of frequency differences caused by sharply localized modifications to stellar structure (*e.g.* Thompson 1988; Vorontsov 1988; Gough 1990), and reflects the variation with frequency in the phase of the eigenfunction at the location of the modification. At the surface the behaviour of the eigenfunction changes slowly with frequency, whereas at greater depth a change in frequency causes the eigenfunction to "sweep through" the point where the model was changed, causing a rapid variation in the frequency change. In the case of the variation of $\mathcal{H}_2$ with ω, Christensen-Dalsgaard & Pérez Hernández (1991) found several cases where the relatively sharp change in Γ_1 in the second helium ionization zone caused an oscillatory behaviour of $\mathcal{H}_2(\omega)$. Similar variations in the basic phase function $\alpha(\omega)$ were analyzed, for example, by Brodsky & Vorontsov (1988b, 1989) and Baturin & Mironova (1990). Vorontsov, Baturin & Pamyatnykh (1992) showed how the phase could be separated in a quantitative fashion into components varying slowly and rapidly with frequency. This type of analysis provides a powerful diagnostic of the properties of the ionization zones of hydrogen and helium, of great interest both for the analysis of the equation of state and for attempts to determine the helium abundance of the solar convection zone.

It is very convenient to express $\mathcal{H}_2(\omega)$ in terms of differences between two models, or the Sun and a model, in a form analogous to equation (5.90). Christensen-Dalsgaard & Pérez Hernández (1992) showed that $\alpha(\omega)$, and hence $\mathcal{H}_2(\omega)$, can be determined directly from the model structure, without computing full modes of oscillation. In this way they were able to find kernels relating $\mathcal{H}_2$ to the model changes. The kernels turn out to be particularly simple if the model changes are expressed in terms of c and the (isothermal) acoustical cut-off frequency

$$\omega_{\rm a} = \frac{c}{2H_p} = \frac{\Gamma_1 g}{2c} \tag{7.154}$$

(*cf.* eq. 5.45). Thus I express $\mathcal{H}_2$ as

$$\mathcal{H}_2(\omega) = \int_{r_0}^{R} \left[K_c(r;\omega)\frac{\delta_r c}{c} + K_{\omega_{\rm a}}(r;\omega)\frac{\delta_r \omega_{\rm a}}{\omega_{\rm a}} \right] {\rm d}r + \mathcal{G}_2(\omega) \; , \tag{7.155}$$

where r_0 is a point suitably deep in the convection zone. Here, as in equation (5.90), the term $\mathcal{G}_2(\omega)$ contains the contributions from the differences (or errors) in the physics of the oscillations: as argued in Section 5.5.3 such errors are likely to be confined very close to the stellar surface and hence probably depend on frequency alone, when properly scaled.

The kernel K_c varies slowly with position and frequency, and hence give little interesting contribution to $\mathcal{H}_2$. On the other hand, the kernels $K_{\omega_{\rm a}}$ have a very distinct behaviour. This is illustrated in Figure 7.16, both as a function of r (at fixed frequency) and as a function of frequency (at fixed r). The r-dependence is qualitatively similar to the behaviour of the scaled eigenfunctions shown in Figure 5.8: the kernels oscillate within an envelope which varies as $c(r)^{-1}$. The frequency dependence clearly illustrates the behaviour discussed above in a qualitative manner: at the surface the kernels vary slowly with frequency (the erratic variations at the lowest frequencies are due to numerical errors), and the variation with frequency becomes increasingly rapid with increasing depth. In fact, as shown by Christensen-Dalsgaard & Pérez Hernández (1992) the kernels may be approximated by

$$K_{\omega_{\rm a}}(r;\omega) \simeq -\frac{1}{c(r)} \cos[2\omega(\tau(r) - \tau')] \; , \tag{7.156}$$

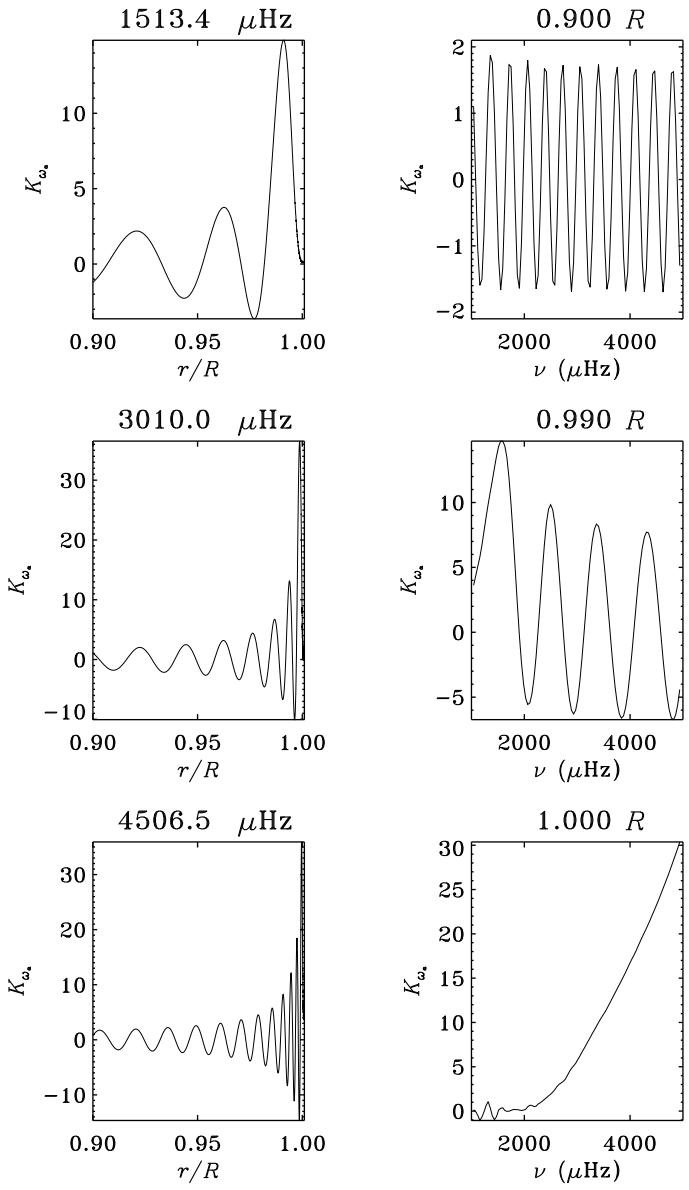

Figure 7.16: The kernels $K_{\omega_a}(r;\omega)$ relating changes in ω_a to $\mathcal{H}_2(\omega)$ (*cf.* eq. 7.155). The left-hand column shows the kernels as functions of r at the frequencies indicated, whereas the right-hand column shows the kernels against frequency, at the radii indicated.

where

$$\tau(r) = \int_r^R \frac{\mathrm{d}r}{c} \tag{7.157}$$

is the acoustical depth, *i.e.*, the sound travel time between the point considered and the surface; also, τ' is roughly a constant. It is evident that according to equation (7.156) K_{ω_a}

is an oscillatory function of ω, oscillating increasingly rapidly with increasing τ and hence increasing depth.

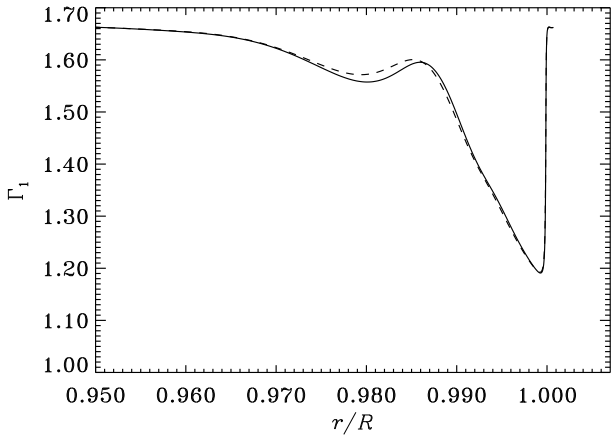

Figure 7.17: The adiabatic exponent Γ_1 in a normal solar model (solid curve) and in a model with helium diffusion and settling (dashed curve).

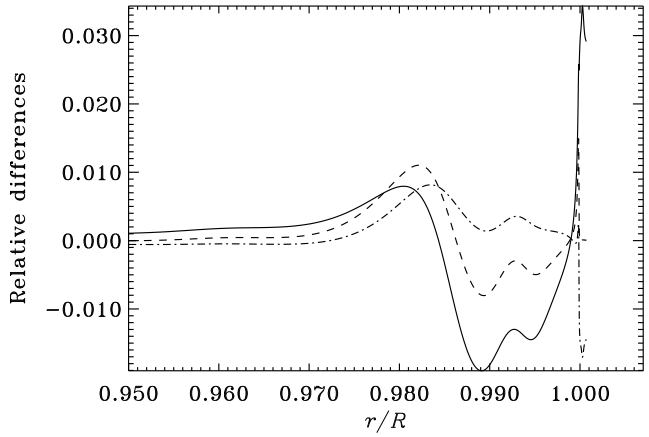

Figure 7.18: Fractional differences between a model of the present Sun with diffusion and a normal model, without diffusion. The solid curve shows $\delta_r c^2/c^2$, the dashed curve $\delta_r \Gamma_1/\Gamma_1$ and the dot-dashed curve $\delta_r \omega_{\rm a}/\omega_{\rm a}$ (*cf.* eq. 7.154).

According to equation (7.155) the variation of $K_{\omega_{\rm a}}$ with ω at a certain r corresponds to the $\mathcal{H}_2(\omega)$ arising from a localized change in $\omega_{\rm a}$ at that position. Hence a sharp feature in $\delta_r \omega_{\rm a}$ at some point $r = r^*$ will give rise to an oscillatory contribution to $\mathcal{H}_2(\omega)$ with a

'frequency' which, from equation (7.156), is approximately $2\tau(r^*)$. Such contributions are in fact clearly visible both in Figure 7.10b, corresponding to the difference between two models differing in the envelope helium abundance, and in Figure 7.13b for the differences between the Sun and a model. The 'frequency' of the variation corresponds to a depth of roughly $0.02R$, *i.e.*, the region of the second ionization of helium.

To understand the origin of this feature I first consider the behaviour of Γ_1. In regions of no or full ionization it is very close to 5/3. However, ionization causes a decrease of Γ_1 below this value; as illustrated in Figure 7.17, there is a major dip in Γ_1 in the overlapping regions of hydrogen and first helium ionization and a smaller, secondary dip in the region of second helium ionization. It is evident that the depth of the second dip must depend on the helium abundance. The effect is clearly visible by comparing the solid curve in Figure 7.17, for the normal nondiffusive model with an envelope helium abundance $Y_{\rm e} = 0.28$, with the dashed curve for the model with diffusion and settling, where $Y_{\rm e}$ has been reduced to 0.25. These effects are also evident in the differences between the two models, shown in Figure 7.18 (the sound-speed difference was also shown in Figure 7.8, but for the whole model). In particular, there is a fairly sharp feature in $\delta_r\omega_{\rm a}$ at $r \simeq 0.985R$, which is responsible for the oscillatory contribution to $\mathcal{H}_2(\omega)$ noted in Figure 7.10b.

These results suggest that $\mathcal{H}_2$ may provide useful information about the properties of the upper parts of the convection zone, including the solar envelope helium abundance which is otherwise quite uncertain. In fact, it was noted in Section 5.1.2 that the structure of the adiabatic part of the convection zone is determined by the composition, in particular the value of $Y_{\rm e}$, as well as the specific entropy s which is essentially constant; in addition, the equation of state must be known. Indeed, the $\mathcal{H}_2(\omega)$ which results from the differences between the observed and the computed frequencies (*cf.* Figure 7.13b) shows oscillations which are superficially quite similar to those resulting from the difference in $Y_{\rm e}$, although overlayed by a substantial slowly varying trend. As shown by Figure 7.16, this slowly varying component approximately corresponds to the contributions that may arise from differences in the outermost parts of the model. More generally, the uncertain physics in the layers immediately below the photosphere and in the solar atmosphere may be expected to give rise to a similar behaviour, as indicated by the function $\mathcal{G}_2(\omega)$ in equation (7.155). This complicates the interpretation of the $\mathcal{H}_2(\omega)$ determined from the observed frequencies. It was shown by Pérez Hernández & Christensen-Dalsgaard (1994a) that the slowly varying part of $\mathcal{H}_2$ can be suppressed in a consistent way through filtering. Furthermore, Pérez Hernández & Christensen-Dalsgaard (1994b) made a fit of the resulting filtered $\mathcal{H}_2$ to models differing in $Y_{\rm e}$ and s, as well as the surface properties; in this way they inferred that $Y_{\rm e} = 0.243 \pm 0.002$. It might be noted that this is quite close to the value obtained in the model with helium settling and diffusion.

The results of such fits, or more generally of any attempt to measure $Y_{\rm e}$ from analysis of solar oscillation frequencies, depend critically on the equation of state. Indeed, all such methods utilize the variation of Γ_1 in the ionization zones; this variation evidently depends on the details of the ionization processes and hence on the thermodynamic properties of the plasma. In fact, Pérez Hernández & Christensen-Dalsgaard (1994b) found that the quality of the fit depended quite sensitively on the assumed equation of state, giving strong preference for one formulation over another, even though both were comparatively sophisticated. This indicates that it may be possible to get some separate information about the composition and the thermodynamic properties of matter in the solar convection zone. However, it is evident that one might conceive of errors in the equation of state with an effect similar

to that corresponding to a change in the helium abundance. Such effects evidently cannot be separated on the basis of an analysis of the oscillation frequencies.

I finally note that the function $\alpha(\omega)$ also enters into the asymptotic behaviour of low-degree modes (*cf.* eq. 7.55); this is visible in the curvature, essentially similar for the different degrees, in the echelle diagram of low-degree solar observations in Figure 2.15. This suggests that it may be possible to obtain information about the near-surface regions, similar to what can be determined from $\mathcal{H}_2(\omega)$, by analyzing observations of stellar oscillations where only modes of degree less than three are generally visible. Brodsky & Vorontsov (1988a) presented a method to determine a function closely related to $\alpha(\omega)$ on the basis of low-degree data alone. This was applied to models of main-sequence stars by Pérez Hernández & Christensen-Dalsgaard (1993), who found a characteristic dependence on the stellar parameters. Further analyses of the effects on the frequencies or frequency separations of the detailed properties of the helium ionization zones were carried out by Monteiro & Thompson (1998) and Miglio *et al.* (2003). A demonstration of the practical utility of this type of analysis, given realistic observational errors and other uncertainties, requires more extensive investigations, however.